



UNIVERSITY OF LEEDS

This is a repository copy of *Simulations of an observed elevated mesoscale convective system over southern England during CSIP IOP 3*.

White Rose Research Online URL for this paper:  
<http://eprints.whiterose.ac.uk/98050/>

Version: Accepted Version

---

**Article:**

White, BA, Blyth, AM and Marsham, JH [orcid.org/0000-0003-3219-8472](https://orcid.org/0000-0003-3219-8472) (2016)  
Simulations of an observed elevated mesoscale convective system over southern England during CSIP IOP 3. *Quarterly Journal of the Royal Meteorological Society*, 142 (698 Part A). pp. 1929-1947. ISSN 0035-9009

<https://doi.org/10.1002/qj.2787>

---

© 2016, Royal Meteorological Society. This is the peer reviewed version of the following article: "White, B. A., Blyth, A. M. and Marsham, J. H. (2016), Simulations of an observed elevated mesoscale convective system over southern England during CSIP IOP 3. *Q.J.R. Meteorol. Soc.*, 142: 1929–1947", which has been published in final form at <http://dx.doi.org/10.1002/qj.2787>. This article may be used for non-commercial purposes in accordance with Wiley Terms and Conditions for Self-Archiving.

**Reuse**

Unless indicated otherwise, fulltext items are protected by copyright with all rights reserved. The copyright exception in section 29 of the Copyright, Designs and Patents Act 1988 allows the making of a single copy solely for the purpose of non-commercial research or private study within the limits of fair dealing. The publisher or other rights-holder may allow further reproduction and re-use of this version - refer to the White Rose Research Online record for this item. Where records identify the publisher as the copyright holder, users can verify any specific terms of use on the publisher's website.

**Takedown**

If you consider content in White Rose Research Online to be in breach of UK law, please notify us by emailing [eprints@whiterose.ac.uk](mailto:eprints@whiterose.ac.uk) including the URL of the record and the reason for the withdrawal request.



[eprints@whiterose.ac.uk](mailto:eprints@whiterose.ac.uk)  
<https://eprints.whiterose.ac.uk/>

# Simulations of an observed elevated mesoscale convective system over southern England during CSIP IOP 3.

White, B.A.

AOPP, Clarendon Laboratory, Department of Physics,  
University of Oxford, Oxford, OX1 3PU, UK

Blyth, A.M.

National Centre for Atmospheric Science (NCAS),  
University of Leeds, UK

Marshall, J.H.

National Centre for Atmospheric Science (NCAS),  
University of Leeds, UK

March 16, 2016

## Abstract

Simulations of an elevated mesoscale convective system (MCS) observed over southern England during the Convective Storm Initiation Project (CSIP) provide the first detailed modelling study of a case of elevated convection occurring in the UK. The study shows that many factors can influence the maintenance of elevated deep convection, from large-scale flow through to surface heating processes and diabatic cooling within the convective system. It is also shown that interactions and feedback mechanisms between a stable layer and the storm can act to maintain deep convection. The simulation successfully reproduced an elevated MCS above a low-level stable undercurrent, with a wave in the undercurrent linked to a rear-inflow jet (RIJ). Convection was fed from an elevated (840 hPa) source layer with CAPE of about  $350 \text{ J kg}^{-1}$ . The undercurrent in the simulation was approximately 1 km deep, about half that observed. Unlike the observed MCS, a transition from elevated to surface-based convection occurred in the simulation due to the combined effects of a pre-existing large-scale  $\theta_e$  gradient, advection and surface heating causing the system to encounter increasingly unstable low-level air and a shallower stable layer that was more susceptible to penetration by downdraughts. The transition to surface-based convection was accompanied by the development of cold-pool outflow and an increase in system velocity from about 6 to  $10 \text{ m s}^{-1}$ . Diabatic cooling from microphysical processes in the simulation enhanced the undercurrent and strengthened the RIJ. This strengthened the wave in the

undercurrent and led to more extensive convection. The existence of a positive feedback process between the convection, RIJ and stable layer is discussed. Uncertainty in the synoptic scale generating errors in the undercurrent is shown to be a major source of error for convective-scale forecasts.

# 1 Introduction

The term “elevated convection” refers to convective clouds where the air parcels feeding the convection originate from above the boundary layer (Glickman, 2000). Here we refer to convection originating from the boundary layer as “surface-based convection”, although purely elevated and purely surface-based convection represent the extreme ends of a continuum of behaviour (Corfidi *et al.*, 2008). Elevated convection can occur in a wide range of environments when instability occurs above any low-level stable layer (e.g. Schmidt and Cotton, 1989; Wilson and Roberts, 2006), above a sloping frontal surface (Colman, 1990; Moore *et al.*, 2003) ahead of fronts (Rochette and Moore, 1996; Browning and Hill, 1984) or above a boundary layer stabilised by surface outflow of cold air from previous convection (Trier *et al.*, 2006; Marsham *et al.*, 2011).

Elevated convection is observed to occur most frequently at night (Fritsch and Maddox, 1981; Wilson and Roberts, 2006), when the nocturnal boundary layer can provide the necessary near-surface stable layer (e.g. Schmidt and Cotton, 1989; Wilson and Roberts, 2006; Marsham *et al.*, 2011). This behaviour has been well-reproduced in both real-data (e.g. Dudhia *et al.*, 1987; Trier *et al.*, 2006) and idealised modelling studies (e.g. Schmidt and Cotton, 1990; Buzzi *et al.*, 1991; Parker, 2008; French and Parker, 2010). Elevated convection has also been observed above daytime stable layers (Browning *et al.*, 2010; Marsham *et al.*, 2010; Browning *et al.*, 2012), although daytime elevated convection is much rarer than nocturnal initiation because strong surface-based instability can occur during the day (Wilson and Roberts, 2006).

Elevated convection may be initiated from unstable air located above the boundary layer (e.g. Marsham *et al.*, 2011), termed “elevated initiation”, but has also been shown to evolve from surface-based convection in observed cases (e.g. Cotton *et al.*, 1983; Wetzell *et al.*, 1983; Corfidi *et al.*, 2008) as well as real-data simulations (e.g. Bernardet and Cotton, 1998; Bernardet *et al.*, 2000; Trier *et al.*, 2006). Likewise, the idealised simulations of (Parker, 2008; French and Parker, 2010) showed an initially surface-based and density-current driven system evolving into an elevated, bore-driven system. Once initiated, elevated convective systems have been observed to evolve into surface-based systems (e.g. Trapp *et al.*, 2001; Bryan *et al.*, 2006; Corfidi *et al.*, 2008; Grim *et al.*, 2009; Marsham *et al.*, 2011; Trier *et al.*, 2011) or may remain elevated throughout their lifetime. However, predicting a transition from elevated to surface-based convection, or vice versa, is difficult because the processes responsible for the transition are difficult to forecast (e.g. the strength and location of convective inhibition (CIN), the location and depth of outflow boundaries, and any change in mesoscale forcing, Corfidi *et al.*, 2008).

It is well-established that lifting at the leading edge of outflow from storms can generate and maintain deep surface-based convection (Charba, 1974; Goff, 1976; Wilson and Schreiber, 1986; Rotunno *et al.*, 1988; Morcrette *et al.*, 2006). Even though elevated convection is characterised by the presence of a low-level stable layer, it is sometimes possible for cold-pool outflow from elevated storms to provide sufficient buoyancy contributions to help maintain convection (e.g. Trier *et al.*, 2006). However, it is rare for elevated convective systems to produce strong surface gusts because it is more difficult for the downdraughts to penetrate through the low-level stable layer and form surface outflow (Corfidi *et al.*, 2008). Lack of secondary initiation from outflow gust fronts has been used to explain the shorter lifetime of elevated storms compared to surface-based storms (Wilson and Roberts, 2006). Whether or not the downdraughts from an elevated storm can reach the surface and form cold-pool outflow depends on the depth and stability of the low-level stable layer (Horgan *et al.*, 2007) as well as on the microphysical processes and environmental humidity that control the strength of diabatic cooling (Blanchard, 1990). Elevated storms can, however, generate waves (e.g. Dudhia *et al.*, 1987; Bosart and Seimon, 1988; Crook and Moncrieff, 1988; Schmidt and Cotton, 1990; Buzzi *et al.*, 1991; Fritsch and Forbes, 2001; Stoelinga *et al.*, 2003; Fovell *et al.*, 2006; Schumacher and Johnson, 2008; Schumacher, 2009; Marsham *et al.*, 2010, 2011) and bores (e.g. Parker, 2008; Marsham *et al.*, 2011) that propagate along the stable layer and provide the lifting required to initiate or maintain deep convection.

Elevated convection is often organised into mesoscale convective systems (MCSs) (Maddox, 1983; Cotton *et al.*, 1989; Laing and Fritsch, 1997). Mature MCSs with a large trailing region of stratiform precipitation (Parker and Johnson, 2000) often develop a system-relative flow of air into the stratiform region from mid-levels at the rear of the system (Smull and Houze, 1985, 1987a,b), likely forming as a dynamic response to heating in the convective line (e.g. Pandya and Durran, 1996). These “rear-inflow jets” (RIJs) provide a supply of dry, potentially cold air from the mid-levels to the convective-scale and system-scale downdraughts and have been observed in both mid-latitude (Houze *et al.*, 1989) and tropical (Chong *et al.*, 1987) squall lines.

The descent and strength of a RIJ has been shown to depend on evaporational cooling (Yang and Houze, 1995; Franklin *et al.*, 2006; Clark *et al.*, 2013a), cooling by melting (Yang and Houze, 1995), cooling by sublimation (Braun, 1995; Braun and Houze, 1997), heating by glaciation (Clark *et al.*, 2013a) and by mid-level moisture (Yang and Houze, 1995), although the relative importance of each of these processes differs between cases and scales (Braun and Houze, 1997; Zhang and Gao, 1989; Yang and Houze, 1995). In some cases the development of an intense RIJ has been linked to the weakening of convection and a dissipation of the system (e.g. Ogura and Liou, 1980; Rutledge *et al.*, 1988; Smull and Houze, 1987b), but in other cases strong convection has been observed for a long time after RIJ formation (e.g. Chong *et al.*, 1987; Houze *et al.*, 1989; Smull and Houze, 1987b). It has been suggested that the descent of a RIJ to the surface can combine with outflow from the convective down-

draughts, thereby increasing convergence along the gust front and maintaining the convective system by triggering new cells (Charba, 1974; Lafore and Moncrieff, 1989). Elevated convective storms have been shown to form RIJs, some of which can descend to the surface (e.g. Schmidt and Cotton, 1989; Trier *et al.*, 2006), and others of which do not (Trier *et al.*, 2006).

Elevated convection frequently produces heavy rainfall (e.g. Rochette and Moore, 1996; Moore *et al.*, 1998, 2003; Wilson and Roberts, 2006) which can sometimes move very slowly (Schumacher, 2009), flash floods (Schumacher and Johnson, 2008), hail (Horgan *et al.*, 2007), and on rare occasion very strong surface winds (Schmidt and Cotton, 1989; Goss *et al.*, 2006; Horgan *et al.*, 2007). Forecasting the initiation of elevated thunderstorms is difficult due to uncertainties in the understanding of the mechanisms that release elevated instability (Moore *et al.*, 2003). Orography and other surface-based forcing features such as boundary layer convergence lines (Bennett *et al.*, 2006) are less important in the initiation of elevated convection than they are in surface-based convection. Instead, the initiation of elevated convection tends to be controlled by features that occur above the surface and boundary layer, such as low-level jets and waves (e.g. French and Parker, 2010; Marsham *et al.*, 2011). Nocturnal storms in the US are poorly forecast compared to storms that occur during the day (Davis *et al.*, 2003), indicating that elevated convection (more likely to occur at night) tends to be difficult to forecast. Precipitation forecasts for cases of elevated convection occurring near a front are also often poor due to the fronts dominating the large-scale dynamical forcing in models and obscuring the forecasts that may otherwise have resulted from elevated initiation (Wilson and Roberts, 2006). Understanding the processes responsible for initiating and maintaining elevated deep convection is therefore crucial for accurate forecasting of the severe weather that can be caused by such storms.

Elevated convection is frequently observed in the US (e.g. Schmidt and Cotton, 1989; Colman, 1990; Moore *et al.*, 2003; Wilson and Roberts, 2006; Horgan *et al.*, 2007; Marsham *et al.*, 2011), particularly in the Southern Great Plains and upper Midwest (Wilson and Roberts, 2006). It is seen much more rarely in the mid-latitude maritime climate of the UK, where the earliest observations were of an MCS which formed ahead of a cold front and above a cool, stable boundary layer (Browning and Hill, 1984). Most recently, a series of elevated MCSs were observed in the daytime in the UK above a low-level stable layer (Browning *et al.*, 2010; Marsham *et al.*, 2010; Browning *et al.*, 2012) on 24 June 2005 during the Convective Storm Initiation Project (CSIP; Browning *et al.*, 2007). Detailed analysis of the structure of the MCS was performed by Browning *et al.* (2010), who identified a RIJ which impacted upon, but did not penetrate, a cold, stable low-level layer and generated a wave (Marsham *et al.*, 2010).

In this paper we present a modelling study of the elevated MCS observed during CSIP. While recent work by other authors has focused on cases of elevated convection occurring in the US (Trier *et al.*, 2011; Marsham *et al.*, 2011), we provide the first known simulations of a case of elevated convection occurring in the UK. The structure and environment of the

observed MCS is summarised in Section 2, but for a full analysis we refer the reader to [Browning \*et al.\* \(2010\)](#) and [Marsham \*et al.\* \(2010\)](#). The high-resolution limited-area model used in this study is described in Section 3, along with the experiment design. The simulation of the case study is presented in Section 4, followed by an investigation into the role of various physical processes in the behaviour of the MCS in Section 5.

## 2 Overview of the 24 June 2005 MCS

Elevated convection occurred during CSIP on 24 June 2005. A series of MCSs remained elevated throughout the intensive observation period (IOP 3). One, referred to as ‘MCS C’ by [Browning \*et al.\* \(2010\)](#), formed off the south coast of the UK on the northern side of a shallow low centred over northern France ([Browning \*et al.\*, 2010](#), their Figure 1). The MCS passed directly over the CSIP region. A tephigram of data from a radiosonde launched ahead and on the southern side of the MCS from Swanage at 1100 UTC. Figure 1a shows that the lowest kilometre of the atmosphere was too cool to feed any deep convective updraughts. However, there were two elevated moist layers: one, centred at 770 hPa (2.3 km), had CAPE of about  $405 \text{ J kg}^{-1}$  provided it could overcome a layer of CIN of  $70 \text{ J kg}^{-1}$  at 740 hPa, while a second moist layer at 870 hPa (1.3 km) had CAPE of  $399 \text{ J kg}^{-1}$  and required greater lifting than the other moist layer to overcome  $263 \text{ J kg}^{-1}$  of CIN before it could undergo deep convection ([Browning \*et al.\*, 2010](#)). The MCS travelled from the southwest to the northeast at a speed of about  $15 \text{ m s}^{-1}$  above a cool low-level stable layer consisting of air flowing from the northeast with a speed of about  $12 \text{ m s}^{-1}$  ([Browning \*et al.\*, 2010](#), their Figures 1 and 4c). This low-level layer flowing strongly against the direction of motion of the MCS was referred to as an “undercurrent”. The convective updraughts were fed from the two elevated moist layers above the undercurrent.

A series of radar scans from the Chilbolton Doppler radar revealed the internal flow structure of the MCS. These scans, along with schematic diagrams summarising the flow structure, can be found in Figures 8 to 13 of [Browning \*et al.\* \(2010\)](#). A major feature was a pair of slantwise updraughts and downdraughts, where one of the slantwise downdraughts was a RIJ. The leading edge of the RIJ impacted on the undercurrent but did not penetrate through it to reach the surface. The impact of the RIJ constricted the depth of the undercurrent, forming a wave ahead of the region of constriction. Detailed analysis of the wave, performed by [Marsham \*et al.\* \(2010\)](#), defined it as a “gravity wave without stagnation” ([Crook and Moncrieff, 1988](#)), since the air in the undercurrent was never at rest relative to the system. [Marsham \*et al.\* \(2010\)](#) determined that the wave provided sufficient uplift to raise both of the elevated source layers to their level of free convection (LFC). No cold-pool outflow was ever observed from the MCS either during the observation period ([Browning \*et al.\*, 2010](#); [Marsham \*et al.\*, 2010](#)), or from further analysis of satellite, radar and surface station observations gathered later in the day.

## 3 Numerical model and experiment design

### 3.1 Numerical model

We used the Advanced Research Weather Research and Forecasting (WRF) model (Skamarock *et al.*, 2008) version 3.1.1 to perform simulations of the 24 June 2005 MCS. WRF is a nonhydrostatic, compressible, 3D atmospheric model. The governing equations in WRF are solved using a time-split integration scheme, allowing slow or low-frequency (meteorologically significant) modes to be integrated using a third-order Runge-Kutta time integration scheme (Skamarock *et al.*, 2008), while the high-frequency (but meteorologically insignificant) acoustic modes are integrated on shorter sub-steps. The spatial discretisation uses Arakawa C grid staggering in the horizontal for the normal velocities and thermodynamic variables. Our configuration used the Morrison two-moment microphysics scheme (Morrison and Khvorostyanov, 2005; Morrison *et al.*, 2009), the Rapid Radiative Transfer Model (RRTM) longwave radiation scheme (Mlawer *et al.*, 1997), the Dudhia shortwave radiation scheme (Dudhia, 1989), the Eta surface-layer scheme (Janjić, 2002) and a thermal diffusion land-surface scheme with 4 soil layers. The Betts-Miller-Janjić (Betts and Miller, 1986; Janjić, 1994, 2000) cumulus parameterisation scheme was used in the outer domain but switched off in the inner domains where the horizontal grid length was fine enough to allow convection to be resolved. No urban physics scheme was used.

At the horizontal grid lengths used in traditional mesoscale models (e.g. 20 km), the scale of turbulence in the model is much smaller than the scale of the spatial filters used on the equations of motion (Wyngaard, 2004). At such scales, no turbulence is resolved and planetary boundary layer (PBL) parameterisations are used to represent subgrid-scale turbulent fluxes. At large-eddy simulation (LES) scales (grid lengths of about 250 m and finer), the scale of the turbulence is much greater than the scale of the spatial filters, and turbulence can be resolved by the model (Wyngaard, 2004). Modern meteorological models are frequently used to perform convection-permitting simulations at grid lengths (e.g. 1 km) where the scale of turbulence starts to approach the scale of the spatial filters. Wyngaard (2004) called this regime the “terra incognita” because neither the PBL parameterisations nor the 3D turbulent mixing and filtering of the model are designed to operate in ranges where the large eddies are partly grid-scale and partly subgrid-scale (Hong and Dudhia, 2012).

PBL parameterisations using local mixing and turbulent kinetic energy (TKE) closure such as the Mellor-Yamada-Janjić (MYJ, Mellor and Yamada, 1982; Janjić, 1990, 1994, 2002) scheme have been shown to have colder and moister biases compared to parameterisations using first-order closure and non-local mixing such as the Yonsei University (YSU, Hong *et al.*, 2006) scheme (Hu *et al.*, 2010; Coniglio *et al.*, 2013). Local PBL schemes (e.g. MYJ) have been shown to produce shallower PBL heights compared to those in non-local (e.g. YSU) schemes (Xie *et al.*, 2012), and have also been shown to represent PBL structures less well (Shin and Hong, 2011). Because the successful reproduction of elevated convection

depends on the representation of the low-level stable layer, and because the simulations presented in this study are performed at a convection-permitting horizontal grid length of 1 km that is within the turbulence “terra incognita” of Wyngaard (2004), we performed a series of tests to check for the best representation of turbulent eddies in our model setup. Although it is beyond the scope of the current paper to perform a sensitivity study of elevated convection to turbulence representation or to boundary-layer parameterisation, we tested simulations using the MYJ PBL scheme, the YSU scheme and with no boundary-layer parameterisation. The three-dimensional structure and evolution of the convection, precipitation and large-scale thermodynamic environment was similar in all simulations. However, both simulations using PBL parameterisations developed stronger boundary-layer heating (which was stronger in MYJ but smoother in YSU) ahead of the storm system than the simulation without a PBL scheme, and were unable to sustain elevated convection for as long. This highlights the importance of being able to represent the boundary layer well, especially as modern convection-permitting simulations often fall into the turbulence “terra incognita” regime. Because of the ability to sustain elevated convection for longer (and because no significant differences in the simulated convection and thermodynamic structure were seen between any of our tests), the simulations we present in this paper are performed without a PBL parameterisation. A full description of the turbulent mixing (prognostic TKE equation) and model filters used in WRF can be found in Chapter 4 of Skamarock *et al.* (2008).

## 3.2 Model domain and initialisation

We used three model nests with a grid ratio of 3:1. The outer domain covered the British Isles and northern France and contained  $173 \times 172$  horizontal grid points with a horizontal grid spacing of 9 km. The inner domain covered southern England and Wales (encompassing the CSIP area) and contained  $535 \times 409$  grid points with a horizontal spacing of 1 km. The standard WRF stretched vertical grid was used, with resolution highest in the lower levels at a spacing of about 100 m near the ground and increasing above the boundary layer. 48 vertical levels were used, sufficient to resolve the low-level stable layer and the RIJ. The model was initialised using initial and lateral boundary conditions generated from Global Forecast System (GFS) analyses starting at 0000 UTC on 24 June 2005. It was not possible to investigate the initiation of the MCS in the simulation because the MCS formed during the model spin-up period (which was about 6 hours). Unfortunately, starting the model earlier could not address this problem because with earlier analyses the model did not reproduce the MCS at all, likely because the low-level stable layer was not represented in the earlier data.

## 3.3 Sensitivity to physical processes

Surface heating was found to erode the low-level stable layer in the control simulation (CTL) so a test was performed in which the surface latent and sensible heat fluxes were set to zero.

Table 1: List of simulations presented in the current paper.

Run	Description
CTL	Full physics simulation
NOSFX	No surface latent or sensible heat fluxes
NOEVP	No contribution to temperature tendency from evaporative cooling
NOSUB	No contribution to temperature tendency from sublimational cooling
NOMLT	No contribution to temperature equation from cooling by melting
NOCOOL	No contribution to temperature tendency from evaporative and sublimational cooling; no contribution to temperature equation from cooling by melting

This simulation, called NOSFX, was otherwise identical to CTL (Table 1).

Diabatic cooling from microphysical processes is known to enhance the RIJ (e.g. Yang and Houze, 1995; Franklin *et al.*, 2006; Clark *et al.*, 2013a). Latent cooling has also been shown to increase maximum vertical velocities, produce a surface gravity current, increase horizontal speeds and reduce upshear tilt (Trier *et al.*, 2011). Marsham *et al.* (2010) suggested that the wave observed in CSIP IOP 3 was formed by the interaction of the RIJ with the low-level stable layer. We therefore tested the influence of diabatic cooling on the properties of the rear inflow and the simulated elevated convection by removing the contribution to the temperature tendency equation from cooling by evaporation (NOEVP, Table 1). Similar simulations were performed with cooling by sublimation (NOSUB) and cooling by melting removed (NOMLT). A final simulation was performed with all diabatic cooling from microphysical processes removed (NOCOOL). The microphysical processes were allowed to occur but the contribution to the temperature tendency and/or the temperature equation was removed. Each of the microphysics tests was otherwise identical to CTL.

## 4 The control simulation

### 4.1 An overview of the control simulation and comparison with observations

#### *The thermodynamic and large-scale structure of the environment*

The vertical thermodynamic structure of the inner model domain from a region just ahead of the simulated MCS at 1100 UTC is shown in Figure 1a compared to data from a sounding made from Swanage, within the inflow to the observed MCS, at 1100 UTC. There was a 50 hPa-deep nearly dry-adiabatic layer near the surface in the simulation surmounted by a moist layer at 840 hPa. This was similar to observations. However, the nearly dry-adiabatic layer in the simulation was shallower than that observed, and the simulation produced a single moist layer that was lower and shallower than the two moist layers in the observations. The simulated and observed values of CAPE in the elevated source layer were 350

and  $405 \text{ J kg}^{-1}$ , respectively.

The cool, nearly dry-adiabatic layer was associated with northeasterly flow of about  $9 \text{ m s}^{-1}$  (Figure 1b). The layer from 1000 hPa to 800 hPa was characterised by strong shear, with winds veering from northeasterly at the surface to southwesterly above 800 hPa (Figure 1b). The low-level northeasterly jet and strong shear in the simulation were comparable to that observed from Swanage, although wind speeds were in general weaker in the model than the observations (Browning *et al.*, 2010, their Figure 4c).

There was surface cold front across Ireland in the outer domain of the model (Fig. 1c) similar to that observed. A gradient in  $\theta_e$  extended across southern England ahead of the cold front such that values of  $\theta_e$  at low levels increased towards the east. The simulated storm formed on the (colder) west side of this gradient, ahead of the front. In addition to the pre-existing  $\theta_e$  gradient, air with large values of  $\theta_e$  was advected from the southeast of the domain (900 to 1260 km E, 0 to 270 km N) towards the UK (Fig. 1c). This process continued throughout the simulation (not shown). At 500 hPa the  $\theta_e$  gradient was weaker and the flow was southwesterly across the whole of the UK (Fig. 1d).

#### *Structure and evolution of the CTL precipitation*

A band of eastward-moving intense precipitation was oriented north to south over Wales and the south-west of England by 0900 UTC in the simulation (not shown), with heaviest precipitation occurring in the south. There was a broad region of less intense precipitation to the west of the band. The observed MCS was poorly organised at 1130 UTC, while the simulated MCS was better organised and located north east of the observed MCS (Figs 2a and b).

By 1430 UTC the structure of the simulated convection was less linear than during earlier stages and had broken up into two large cells joined by a region of stratiform precipitation (Fig. 2c), whilst the radars observed a line of intense convection oriented approximately SSW-NNE (Fig. 2d). Despite this difference, there was reasonably good agreement between the simulated and observed MCS at 1430 UTC. Two significant changes in the behaviour of the simulated MCS occurred between 1300 and 1400 UTC: the westerly component of the system velocity became greater than at previous times and the system speed also increased (Section 4.2).

A series of intense cells formed in the east of the domain ahead of the MCS at 1430 UTC (Fig. 2c). These were not present in the observations. It will be shown later that these formed along an outflow boundary from the convection. The simulated MCS continued to move eastwards, eventually merging with these smaller cells, leaving the east coast of the UK by 1800 UTC and weakened over the sea until it fully dissipated by 2000 UTC (not shown). This was consistent with the observed system.

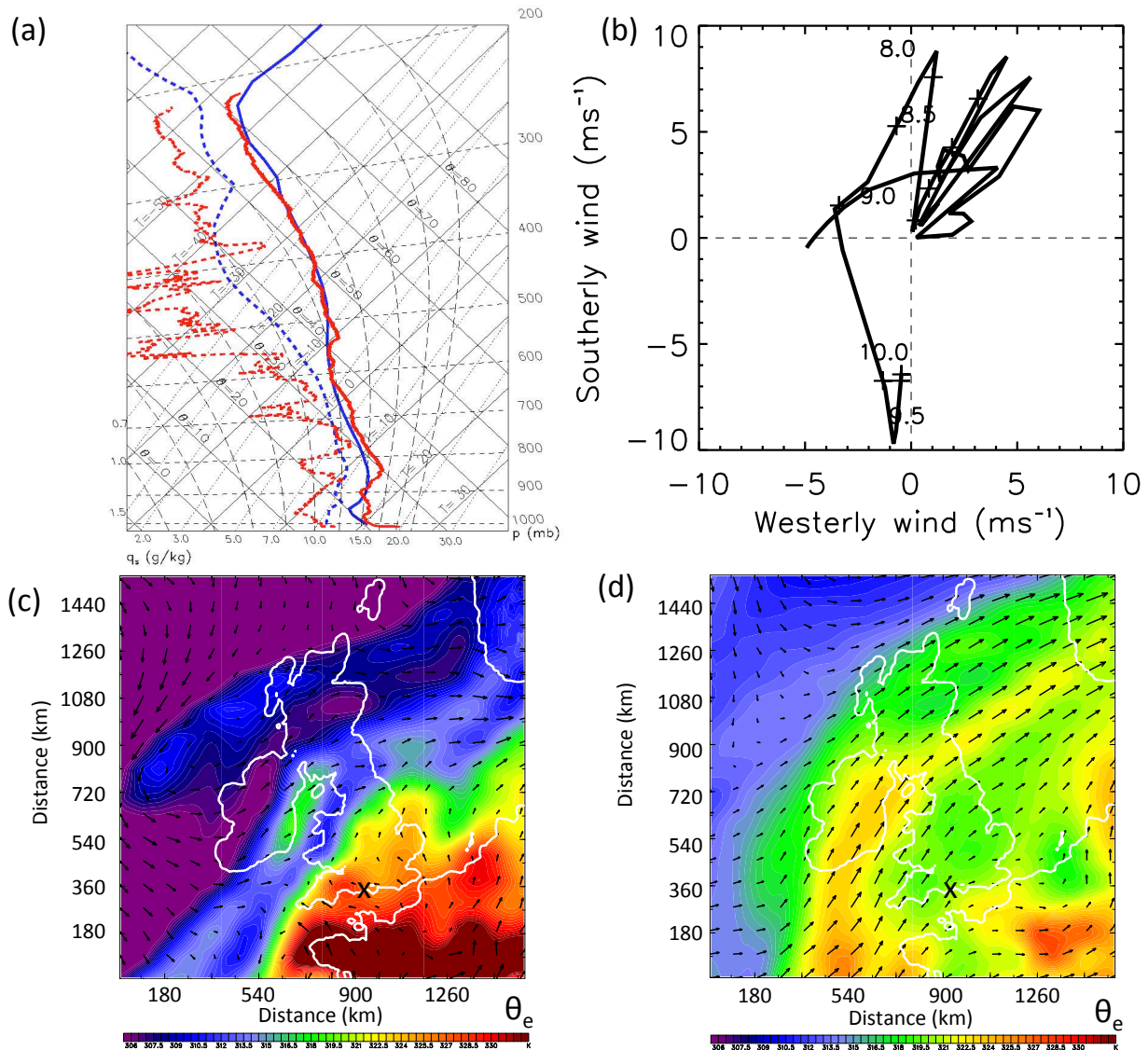


Figure 1: (a) Tephigram constructed from model data ahead of the CTL MCS at 1100 UTC 24 June 2005 (blue line). Also shown is the Swanage 1100 UTC 24 June 2005 sounding (red line), which is shown in Fig. 4a in [Browning \*et al.\* \(2010\)](#). Short dashed black lines are isobars, long dashed black lines are saturated adiabats, dotted lines are lines of constant saturated specific humidity and solid black lines are dry adiabats. (b) wind hodograph showing the simulated wind profile at Swanage, with pressure in the lower levels labelled in hundreds of hPa. (c, d) 900, 500 hPa  $\theta_e$  (K, colour contour) and horizontal wind vectors from the model at 0000 UTC 24 June 2005. Horizontal distances are in km. Swanage is marked with a black 'x'.

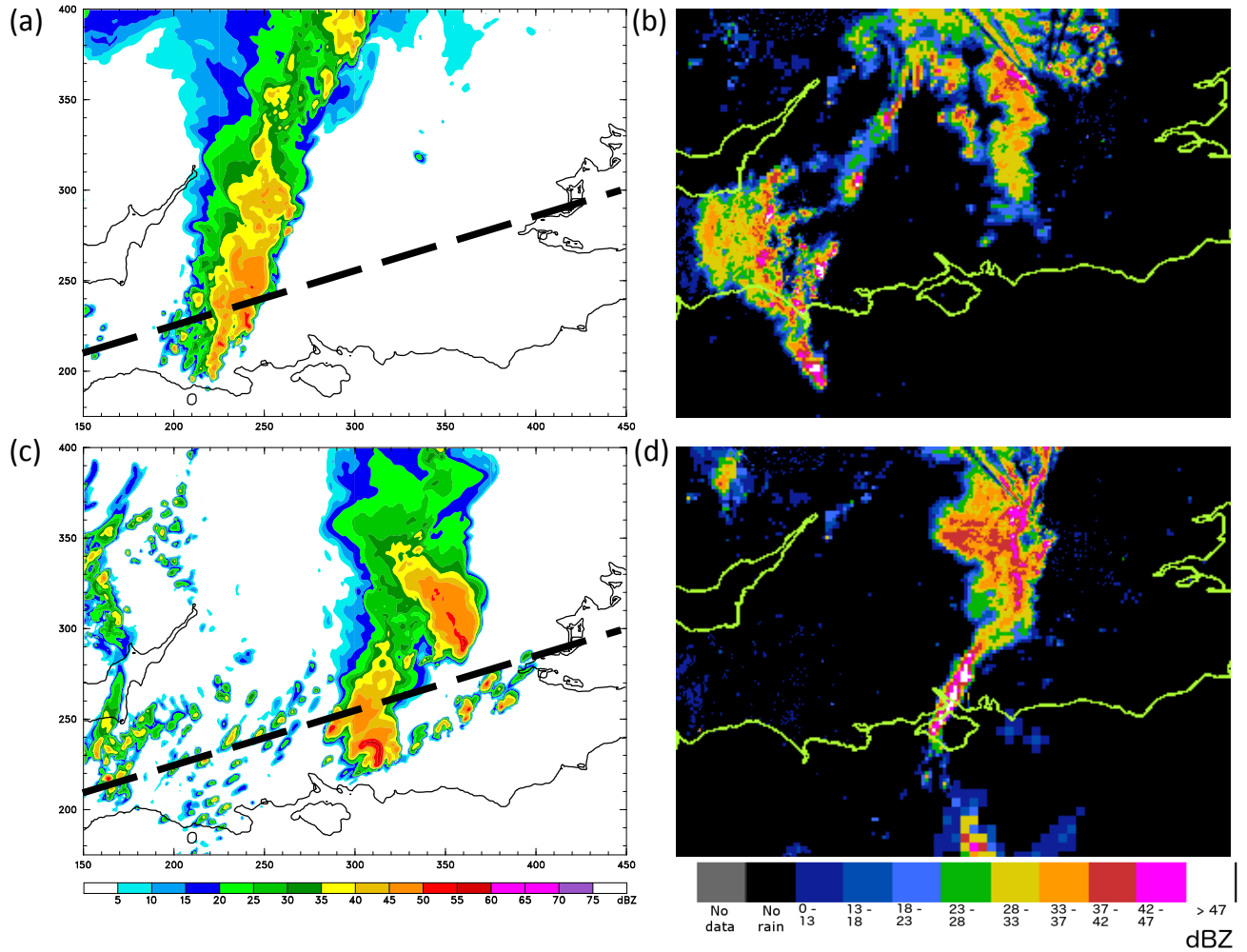


Figure 2: (a,c) Simulated reflectivity (dBZ) from the inner domain (1km horizontal grid spacing) of the CTL simulation for 24 June 2005 and (b,d) observed reflectivity (dBZ) from the NIMROD network rain radar. Data are shown at (a,b) 1130 and (c,d) 1430 UTC. Black dashed lines on the simulated reflectivity field indicate the lines along which vertical sections were made. The island at 290 km E and 190 km N is the Isle of Wight.

## 4.2 Evolution of the control simulation

### *CTL system velocity*

The velocity of the simulated MCS increased between 1300 and 1400 UTC (Fig. 3). A Hovmöller diagram of vertical velocity and column-integrated cloud made east to west at a height of about 2.3 km is presented in Figure 3. This height corresponds approximately to the height of both the rear inflow and of the elevated inflow layer (shown later in Fig. 4), and the up- and downdraughts therefore correspond to the passage of the elevated inflow and the rear inflow, respectively. Cloud formed during the spin-up period of the simulation and consolidated at about 0600 UTC, at which time an updraught of about  $2 \text{ m s}^{-1}$  formed and preceded a downdraught of about  $-2 \text{ m s}^{-1}$ . The convective system propagated across the domain at a reasonably constant speed of about  $6.4 \text{ m s}^{-1}$  until 1330 UTC, and increased in speed to about  $10.3 \text{ m s}^{-1}$  thereafter (Fig. 3). A series of intense ( $5 \text{ m s}^{-1}$ ) updraughts developed some time after the increase in speed. It will be shown that the increase in system velocity coincided with a transition from elevated, wave-forced convection with no cold outflow reaching the surface, to a phase where cold outflow reached the surface once the convection became surface-based.

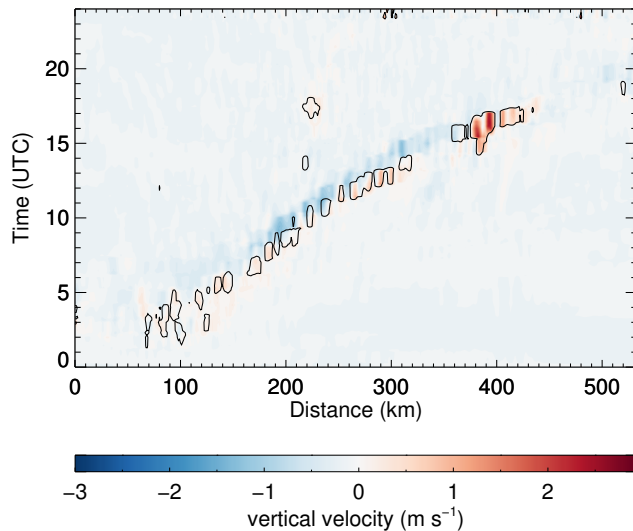


Figure 3: Hovmöller diagram along the centre of the southernmost region of the MCS showing vertical velocity ( $\text{m s}^{-1}$ , colour contour) and column-integrated cloud at  $2.0 \text{ g kg}^{-1}$  (black line contour) at a height of 2.3 km.

### *Vertical structure of the CTL MCS and its environment*

The vertical structure of the convection and its near-environment evolved considerably throughout the simulation. Figure 4 is a series of vertical sections of equivalent potential temperature ( $\theta_e$ ), system-relative winds resolved along the plane of the section and total cloud mixing ratio made at different times through the inner model domain. These sections were made through the centre of the southernmost region of the MCS and approximately

normal to the orientation and direction of motion of the storm, along the line shown in Figure 2, and are averaged 10 km into and out of the plane of the vertical section. At 0730 UTC the main convective region of the MCS was located between 40 and 70 km, with a stratiform anvil region extending back to 10 km and forwards to 260 km (Fig. 4a). The MCS propagated rightwards along this section, from the southwest to the northeast. A significant feature of the early pre-convective environment was a low-level, low-valued  $\theta_e$  layer in the lowest 1 km between 0 and 160 km (Fig. 4a). The air making up this layer flowed against the direction of motion of the MCS and was similar to the undercurrent associated with MCS C, described by Browning *et al.* (2010, their Figure 8c). We henceforth use the term ‘undercurrent’ to refer to the low-level layer of cool air flowing against the MCS. Above the cold undercurrent and ahead of the simulated MCS there was an elevated layer of high-valued  $\theta_e$  (328 to 330 K) centred at a height of 2 km. This air was the source air for the convection (Fig. 4a). To the rear of the convective system there was inflow between heights of 3.5 and 6.0 km which descended under the rear stratiform region bringing low-valued  $\theta_e$  air down to 1 km (Fig. 4a). The descending rear-inflow did not penetrate through the undercurrent at that time, as there were no system-positive winds anywhere at the surface (Fig. 4a). We will show in more detail that the descending rear inflow constricted the undercurrent and formed a wave at the top of the undercurrent and in the elevated source layer, similar to the RIJ in the observations. Even at the scale shown in Fig. 4a, cloud can be seen in the elevated source layer just ahead of the rear inflow (80 km, at heights of 2.0 to of 3.5 km) indicating that air in the wave was lifted to its condensation level.

There were four distinct waves at the top of the undercurrent and in the elevated source layer at 0815 UTC (Fig. 4b), caused by the constriction of the undercurrent by the RIJ. We note that the wave-like feature in the undercurrent must be a wave and not a bore because the flow within the undercurrent and the elevated source layer is towards the stepwise decrease in flow height, not away from it (Parker, 2008; French and Parker, 2010).

Finer-scale detail of the airflow and the waves in the elevated layer is given in Fig. 5a, which focuses on the region in Fig. 4b in the lowest 4 km from 50 to 150 km. Four waves in the top of the undercurrent and in the elevated source layer had peaks at 27, 33, 43 and 50 km, giving an average wavelength of about 7.5 km. This compares well to the 7 km wavelength observed by Marsham *et al.* (2010). The first wave (at 27 km) formed just ahead of the nose of the RIJ, which descended to 1.2 km. Each of the wave peaks in the elevated source layer was associated with ascent and the formation of shallow cloud (Fig. 5a). The RIJ descended within a stratiform precipitation region (Fig. 5a). It will later be shown that diabatic cooling from microphysical processes strengthened the descent of the simulated RIJ. The airflow in the RIJ, the undercurrent, the elevated source layer, the waves in the source layer, and regions of liquid cloud, graupel and rain are synthesised in the diagram shown in Fig. 5b. The cool undercurrent is shown flowing against the MCS in the lowest 1 km. The RIJ descends through a region of graupel to the top of the undercurrent, and the elevated source layer (at a height of about 2 km) flows towards the storm. Wave peaks form at the top

of the undercurrent and in the elevated source layer where the RIJ meets the undercurrent but does not penetrate through. The ascent in these waves in the source layer (wind vectors, Fig. 5a) is associated with the formation of cloud at each of the peaks.

Values of  $\theta_e$  increased significantly at low-levels between 0815 and 1015 UTC. Ahead of the MCS in the region between 200 and 300 km, high values of  $\theta_e$  extended from the surface to about 750 m at 1015 UTC (Fig. 4c). Values of  $\theta_e$  also increased in the undercurrent near the MCS and in the elevated source layer feeding the storm (Fig. 4b). Because the source layer was centred at a height of 2 km (and no instantaneous-mixing PBL scheme was used) this increase could not have been due to surface heating and was therefore likely due to advection (Fig. 1c). The descent of the RIJ stopped at the top of the undercurrent, and the wave in the elevated source layer and cloud associated with the wave remained (Fig. 4c).

Strong near-surface and boundary layer heating ahead of the MCS continued between 1015 and 1130 UTC. Particularly significant and deep increases in  $\theta_e$  occurred between 230 and 300 km, with values greater than 332 K originating from the surface and extending to a height of about 1.5 km (Fig. 4d), as well as in a layer at a height of about 1 km just above the undercurrent. Again, this increased  $\theta_e$  above the surface was at least in part due to advection (Fig. 1c). The flow from this region of strongly increased  $\theta_e$  was towards the storm (Fig. 4d), indicating the potential for a transition from elevated to surface-based convection to occur as the MCS propagated to the northeast (rightward along the section) through the elevated source layer towards the region of high-valued  $\theta_e$  originating from the surface. Although there were higher values of  $\theta_e$  in the undercurrent by this time, and hence it was somewhat weakened, the RIJ did not descend through it, and the wave in the elevated source layer and cloud associated with the wave were still present (Fig. 4d).

The MCS had passed through the elevated source layer and into the region of high-valued  $\theta_e$  air originating from the surface by 1330 UTC (Fig. 4e), suggesting that the inflow to the convection was entirely surface-based by this time. The completion of this transition coincided with the increase in system velocity (Fig. 3), and the depth of the potentially warm layer extended from the surface to a height of more than 2 km (Fig. 4e). The RIJ could not be seen to undergo any significant descent at this time. Very little of the undercurrent remained, with a layer of low-valued  $\theta_e$  extending from the surface to a height of about 1.5 km at 220 km (Fig. 4e). However, this was deeper than the undercurrent at this location at previous times (Figs 4a-d), and so it is likely that at least some of this potentially cold air was supplied from either or both of the convective downdraughts or the RIJ.

The MCS, centred at 220 km and with anvil extending from 200 to 250 km, appeared cut off from the surface-based source layer along this particular (10 km averaged) vertical section at 1430 UTC (Fig. 4f). However, the inflow was surface-based along other sections of the MCS at this time (not shown). Significant cold-pool outflow formed by 1430 UTC, with  $\theta_e$  values less than 321 K about 750 m deep between 220 and 280 km (Fig. 4f). Part

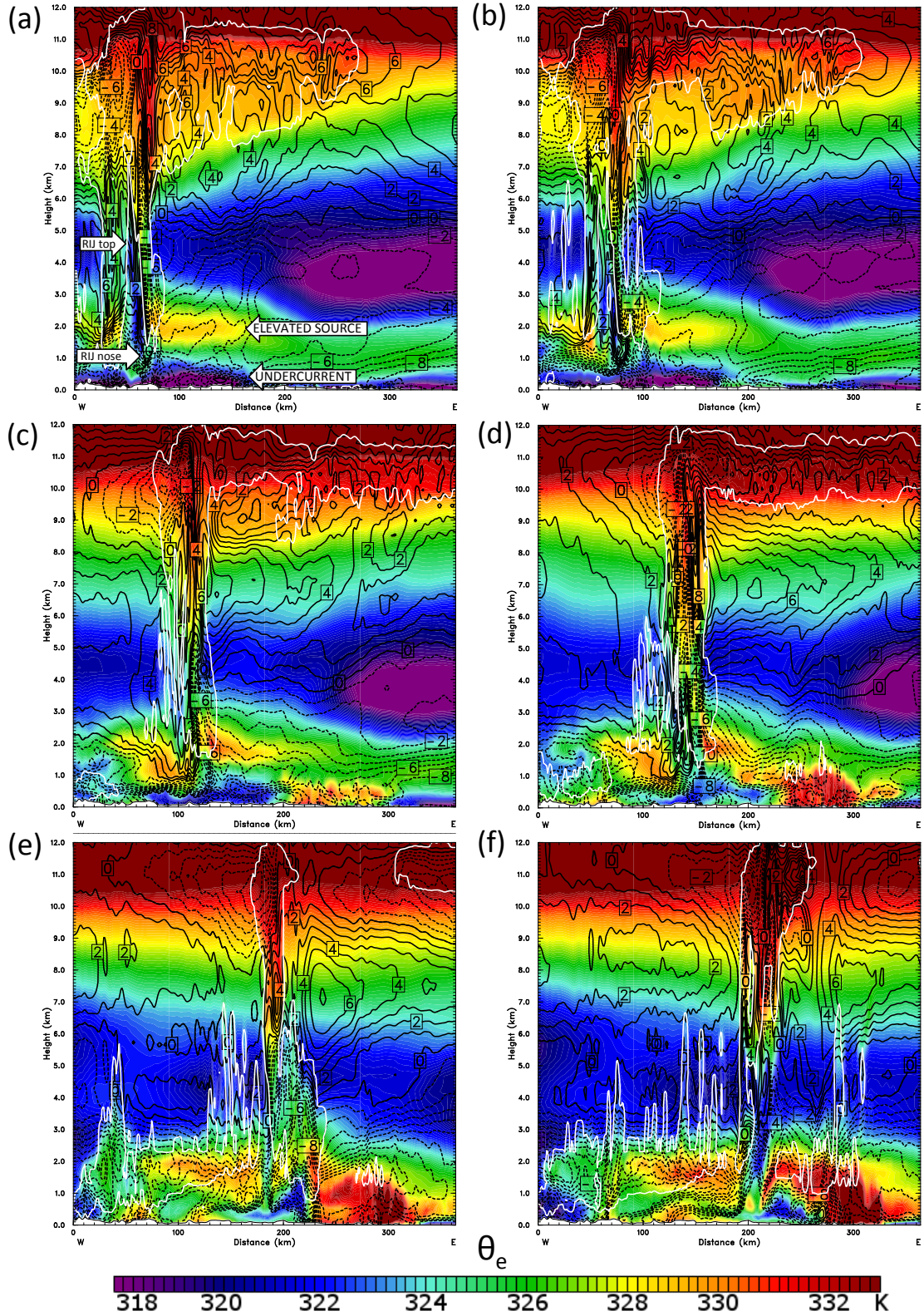


Figure 4: Vertical sections through the inner domain (1 km horizontal grid spacing) of the model showing  $\theta_e$  (K, colour contour), system-relative horizontal winds ( $\text{m s}^{-1}$ , solid black line contour showing positive system-relative winds and dashed black line contour showing negative system-relative winds) and a single contour of the total value of the cloud water and ice mixing ratios ( $5 \times 10^{-3} \text{ g kg}^{-1}$ , white line contour) at (a) 0730, (b) 0815, (c) 1015, (d) 1130, (e) 1330 and (f) 1430 UTC. Labelled arrows indicate the top and nose of the rear inflow jet (RIJ), elevated source and undercurrent in (a).

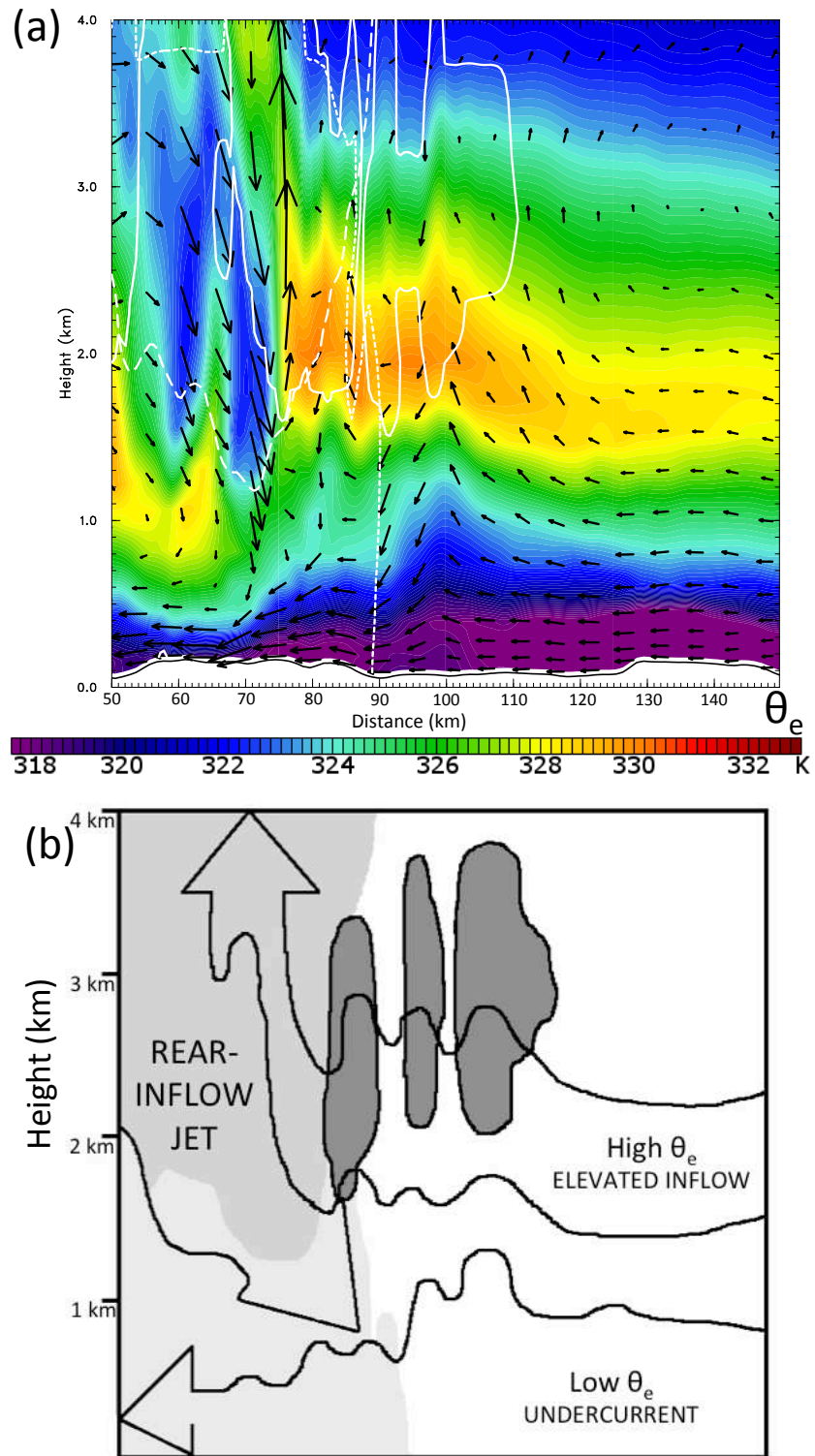


Figure 5: (a) Detail of the region from heights of 0 to 4 km from 50 to 150 km in Fig. 4b at 0815 UTC, showing  $\theta_e$  (colour contour), system-relative 3D wind vectors resolved along the plane of the section and also showing a contour of the  $5 \times 10^{-3} \text{ g kg}^{-1}$  cloud, graupel and rain mixing ratio (solid, dashed and dotted white lines, respectively). (b) Schematic diagram showing the airflow in (a) and with shading showing regions of liquid cloud in dark grey, graupel in mid grey and rain in light grey. Note that the origin of Fig. 5a corresponds to 50 km in Fig. 4b

of the reason that the MCS appeared cut off from its inflow was that the low-valued  $\theta_e$  air in the region between 1.5 and 5 km immediately beneath the MCS (Fig. 4f) was part of a large downdraught with descent stronger than  $5 \text{ m s}^{-1}$  that was contributing to the cold-pool outflow (not shown).

The RIJ did not undergo significant descent at this time, only reaching a height of about 2 km at 215 km (Fig. 4f). However, it is also possible that the RIJ was continuing to feed the intensifying downdraught (without any significant system-relative forward motion) which, because of its strength, was almost vertically orientated below 2 km. The surface outflow penetrated through the region of high-valued  $\theta_e$  air extending from the surface to 2.5 km ahead of the main convective cell (Fig. 4f). There were system-positive winds at the front of the cold-pool outflow in the lowest 500 m at 270 km (Fig. 4f). Above the system-positive flow in the cold pool, cloud formed with a base height of about 1 km and reached a height of about 7 km just ahead of the outflow (Fig. 4f). The sequence of plan views (Fig. 2) and cross-sections (Fig. 4) show that the cells of precipitation ahead of the MCS in Fig. 2e were therefore new convective cells that formed along an outflow boundary from the original MCS.

Vertical sections of CAPE and CIN shown in Fig. 6 confirm the transition from elevated to surface-based convection at about 1330 UTC. At 0730 UTC, the highest values of CAPE were found in the elevated layer located between heights of 1 and 3 km ahead of the MCS (Fig. 6a). The layer continued to have highest values of CAPE as the storm propagated through it at 0815 UTC (Fig. 6b). Although it remained the source layer of the convection at 1015 UTC, it can be seen that high CAPE values were developing in the near-surface layer ahead of the storm between 200 and 300 km (Fig. 6c). The near-surface layer continued to deepen as the MCS propagated towards it (Fig. 6d), and at 1330 UTC the MCS had nearly passed through the entire elevated layer with high CAPE and reached the near-surface high CAPE layer (Fig. 6e). By 1430 UTC, there was no evidence of an elevated layer with high CAPE, and rather the highest CAPE values occurred in the 2 km extending from the surface, indicating the completion of the transition from elevated to surface-based convection (Fig. 6f).

Trajectories calculated 2 hours backwards from 0815 UTC and initialised in the undercurrent and in the RIJ show that air in the RIJ did not penetrate through the undercurrent during the elevated convection stage (Fig. 7a). The heads of the trajectories correspond to the time of the vertical section of  $\theta_e$ , wind vectors and cloud that the trajectories are plotted over. Fig. 7a shows that some portion of the air from the RIJ descended with the main downdraught and turned back on itself into (and with the flow of) the undercurrent, but none of the descending air from either the RIJ or the main downdraught had any forward component of flow that penetrated through the undercurrent.

By 1330 UTC in the CTL simulation (the transition stage from elevated to surface-based convection and the time at which cold pool development first occurred), 2-hour back trajec-

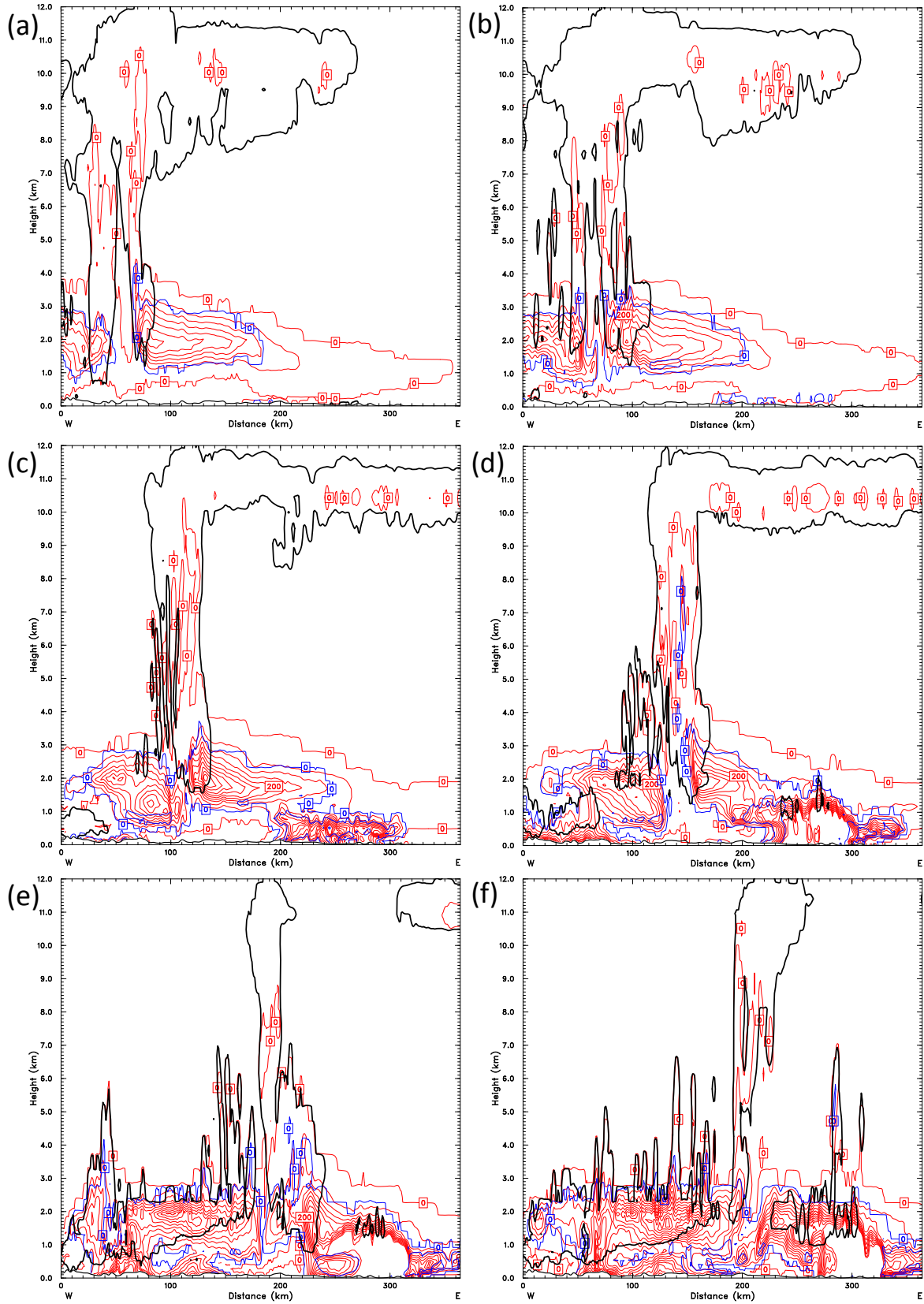


Figure 6: Vertical sections similar to those in Fig. 4 through the inner domain (1 km horizontal grid spacing) of the model showing CAPE (red line contour), CIN (blue line contour) and total cloud water and ice mixing ratios ( $5 \times 10^{-3} \text{ g kg}^{-1}$ , black line contour) at (a) 0730, (b) 0815, (c) 1015, (d) 1130, (e) 1330 and (f) 1430 UTC.

tories show that the air in the cold outflow between the surface and 600 m originated partly from anti-system flow in the undercurrent, and partly from the descent of the RIJ (Figure 7b). Therefore, at the transition stage, some of the air in the surface outflow was from the RIJ. However, parts of this contribution to the cold-pool outflow turned back against the direction of motion of the MCS and strengthened the undercurrent rather than contributing to the cold pool.

At 1430 UTC, 3-hour back trajectories to identify the origin of the air in the convective downdraughts and the origin of air in the cold pool show that by this time the RIJ was partially feeding the downdraughts (which in turn would feed the cold pool) and partially feeding the cold pool directly by penetrating to the surface (Figure 7c).

*The relationship between the strength of the CTL gravity current outflow and the low-level shear*

Cold pool outflows from storms can often be described by gravity current theory (e.g. Simpson, 1969; Charba, 1974; Mueller and Carbone, 1987; Wakimoto, 1982). The theoretical propagation speed  $c$  of a gravity current propagating in a fluid of infinite depth is given by

$$c^2 = -2 \int_{z=0}^{z=H} B dz, \quad (1)$$

where  $H$  is the depth of the gravity current and  $B = g(\theta'_v/\bar{\theta}_v - q_L)$  is the total buoyancy including contributions from the virtual potential temperature perturbations,  $\theta'_v$ , and the mixing ratio of all condensate,  $q_L$  (Simpson, 1969; Trier *et al.*, 2006). The speed of a gravity current is often referred to as its strength. It is well-known that lifting at the gust front of a cold pool can initiate deep convection (e.g. Lin *et al.*, 1998). The most recent form of RKW theory (Weisman and Rotunno, 2004) states that an optimal state for the maintenance of deep convection in a shear environment can exist when the relative strength of the circulation associated with the cold pool is balanced by the circulation associated with the ambient shear in the lowest 5 km, i.e. when the ratio of the cold pool strength to the shear,  $c/\Delta u$ , is between 1 and 1.5. (We note that the earliest form of RKW theory, Rotunno *et al.* (1988), used the horizontal buoyancy in the lowest 2.5 km, but that the theory was later updated to its current form by Weisman and Rotunno (2004) to use the depth of the horizontal buoyancy in the lowest 5 km AGL). In this state, the effect of the cold pool on tilting the updraught to the rear is balanced by the tendency of the updraught to tilt downshear, so updraughts can be maintained for longer than in the case of either a shear environment without a cold pool, or a cold pool in the absence of environmental shear (Rotunno *et al.*, 1988).

The simulated MCS formed a surface cold-pool outflow in the later stage of its lifetime. This appeared to occur after the convection became surface-based (Fig. 4e), and in an environment with strong shear due in part to the presence of the low-level flow against the motion of the MCS. There is however an alternative interpretation: perhaps the cold pool formed first, just before the surface-based air started feeding the MCS. The order in which

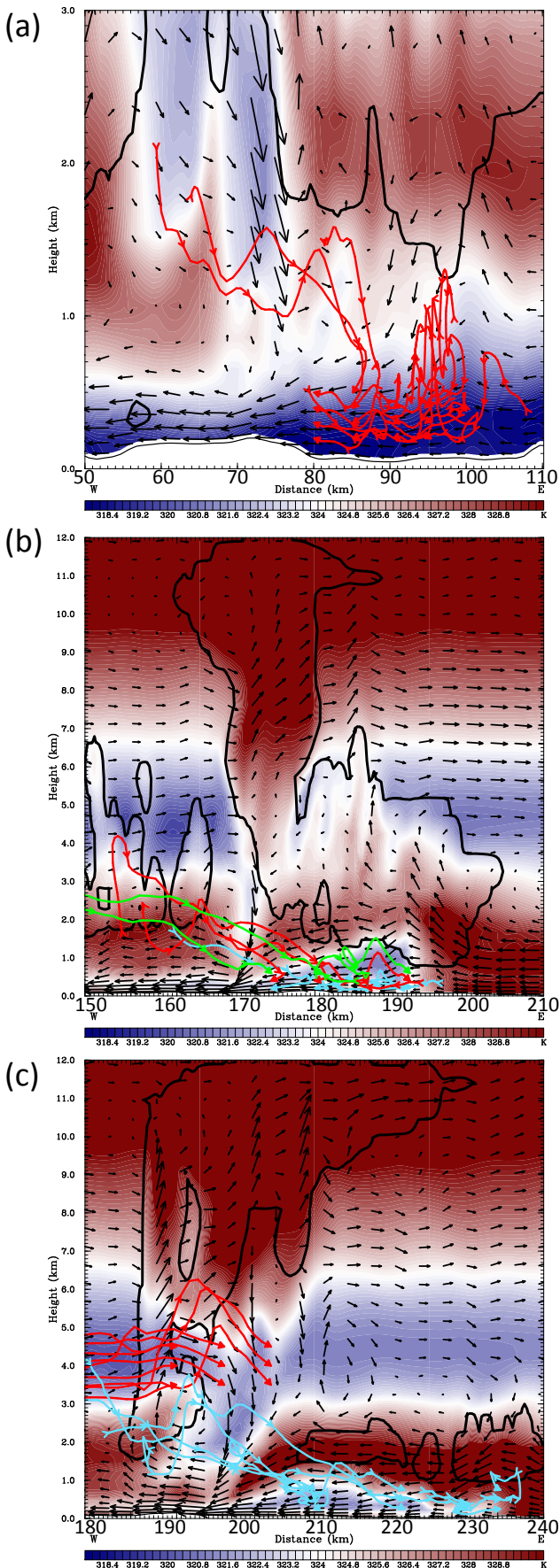


Figure 7: Back-trajectories (red, cyan and green lines) overlapped on  $\theta_e$  contours (red-blue colour contours), total cloud water and ice mixing ratios ( $5 \times 10^{-3} \text{ g kg}^{-1}$ , black line contour) and 3D wind vectors resolved along the plane of the vertical section at (a) 0815 UTC, with red trajectories initialised in the undercurrent at 80, 85, 90, 95 km and in the RIJ at heights of 200, 300, 400 and 500 m, along the plane of the vertical section in Fig. 4b, (b) 1330 UTC, initialised from 190, 200, 210 and 220 km along the vertical section shown in Fig. 4e at heights of 200 (cyan), 400 (red) and 600 m (green), and (c) 1430 UTC, initialised in the downdraughts from 200, 210 and 220 km at 3.5, 4.0 and 4.5 km along the vertical section in Fig. 4f (red trajectories), and in the cold pool at 30, 250 and 270 km at 250, 500 and 750 m along Fig. 4f (cyan trajectories). Note the difference in vertical scale between (a) and (b,c). Also note that the horizontal scales of the individual panels correspond to the horizontal axis in Figure 4.

the cold pool and low-level flow formed cannot be determined at the 15-minute temporal resolution of our high-spatial resolution data. Regardless, the generation of the cold pool meant it was of interest to describe the cold-pool outflow as a gravity current and to see whether the RKW optimal state condition was met. In calculating the cold-pool buoyancy along the cross-section shown in Fig. 4 for use in Equation 1, it was noted that the air was not saturated at low levels either inside or ahead of the gravity current, so the contribution from the condensate and water vapour could be ignored. The water vapour mixing ratio inside the gravity current was the same as that in the environment, so when calculating  $\theta'_v$ , the  $q$  term could be ignored and the value of  $\theta_v$  in Equation (1) could be assumed to be the same as  $\theta$ .

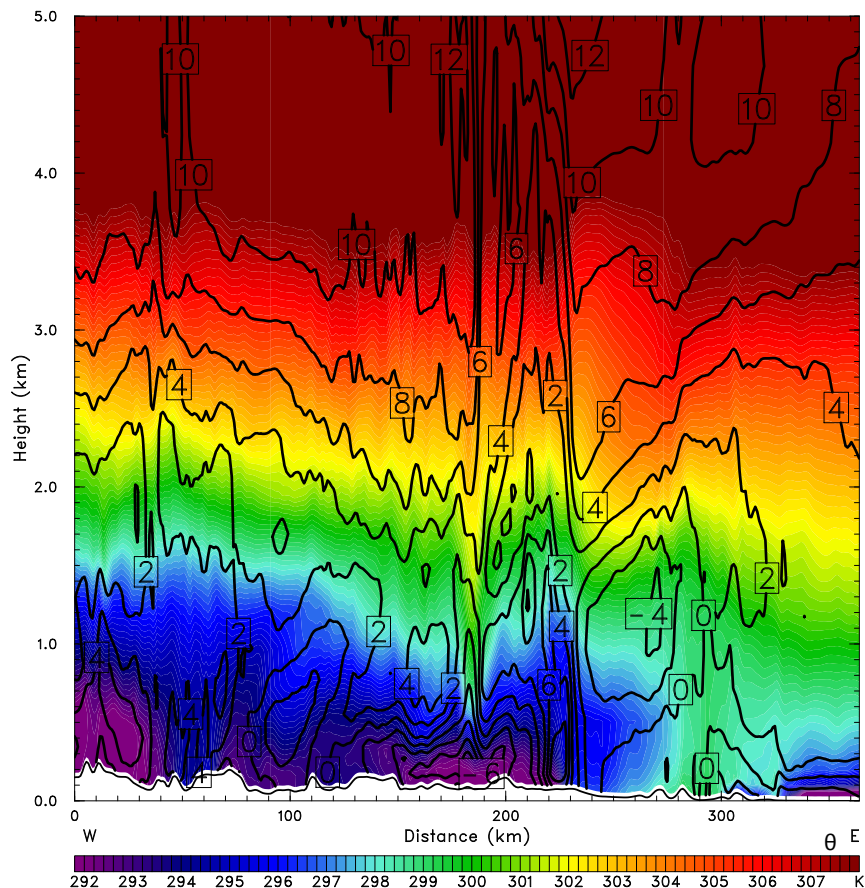


Figure 8: Vertical section as Fig. 4 showing  $\theta$  (K, colour contour) and horizontal winds (not system-relative) from heights of 0 to 5 km at 1330 UTC

The depth of the outflow with  $\theta$  less than 294 K between 200 and 230 km at 1330 UTC was about 650 m and the potential temperature perturbation between the outflow and the environment ranged between 4 and 7 K, depending on the height at which it was defined (Fig. 8). The environmental potential temperature was between 297 and 300 K (Fig. 8). These val-

ues gave a range of instantaneous gravity current strengths,  $c$ , from 13.1 to 17.3 m s<sup>-1</sup>, consistent with gravity current speeds calculated from the 15-minute model output of 13.9 and 16.7 m s<sup>-1</sup> at 1330 and 1430 UTC, respectively (not shown). Here we use the range of instantaneous gravity current strengths at 1330 UTC because we are interested in the potential for deep lifting as soon as the cold pool formed. The pre-convective environment in the simulation was characterised by strong shear: the system-relative flow at low-levels was towards the MCS, while that at mid- and upper-levels was away from the MCS (Fig. 4). The vertical shear of the horizontal velocity in the lowest 5 km ahead of the system was 13 m s<sup>-1</sup> (Fig. 8), giving a range of  $c/\Delta u$  values from 1.3 to 1.0. This was consistent with the “optimal state” criteria of Weisman and Rotunno (2004) for deep lifting at the leading edge of the gravity current. The Hovmöller diagram of vertical velocity (Fig. 3) and the series of vertical sections (Fig. 4) show that the velocity of the MCS increased when the transition from elevated to surface-based convection occurred and the system produced cold-pool outflow (similar to the findings of Parker, 2008; French and Parker, 2010, who showed a change in system speed with a change in forcing mechanism). Because the strength of the gravity current and the environmental shear met the “optimal state” criteria for deep lifting, it is possible that the strength of the outflow may have helped to maintain deep convection in the shear environment of the simulation.

#### Summary of the behaviour of the CTL MCS:

- Elevated convection formed above an undercurrent.
- A RIJ formed, which descended but initially did not penetrate through the undercurrent.
- Waves formed in the top of the undercurrent ahead of the RIJ, and air was lifted in the wave.
- The MCS propagated through a pre-existing large-scale  $\theta_e$  gradient towards more buoyant air in the east.
- In addition to the pre-existing gradient, air at low-levels became increasingly buoyant throughout the simulation, leading to both the weakening of the undercurrent and the development of very buoyant near-surface air ahead of the MCS.
- A transition from elevated to surface-based convection occurred when the MCS had propagated through the elevated inflow layer and reached the region of buoyant near-surface air.
- As the transition to surface-based convection occurred, air from the RIJ was able to penetrate to the surface.
- After the transition to surface-based convection occurred, cold outflow formed from the storm.

Table 2: Magnitude of the velocities of the simulated MCS. In simulations where two system velocities were seen, these correspond to different stages in the evolution of the MCS. In such cases we use  $v_1$  to refer to the velocity in the first stage of the MCS lifetime and  $v_2$  to the velocity in the later stage of the MCS lifetime. In simulations where no change in system velocity was seen, the single velocity of the MCS is referred to as  $v_1$ .

Run	$v_1$ (m s <sup>-1</sup> )	$v_2$ (m s <sup>-1</sup> )
CTL	6.4	10.3
NOSFX	5.8	9.4
NOEVP	6.1	
NOSUB	5.1	
NOMLT	6.5	12.4
NOCOOL	7.2	

- Once cold outflow formed, the ‘optimal state’ criteria of [Weisman and Rotunno \(2004\)](#) for deep lifting were met.
- The development of cold outflow coincided with an increase in speed of the MCS.

## 5 The dependence of the MCS on selected physical processes

### 5.1 The dependence of the MCS on surface heat fluxes: NOSFX

#### *The structure and evolution of the simulated precipitation*

To test the effect of surface heating on the evolution of the convection, we removed the surface latent and sensible heat fluxes from the model. Zonally-averaged Hovmöller diagrams are shown in Figure 9, and the system velocities are summarised in Table 2. Like CTL, the NOSFX MCS had two different speeds, corresponding to two stages of its evolution: an initially slower speed of 5.8 m s<sup>-1</sup> until about 1330 UTC, when its speed increased to 9.4 m s<sup>-1</sup>. These speeds were slightly slower than, but close to, those of CTL (Table 2), but both system velocities were slower than those of the observed MCS which had an initial speed of 15 m s<sup>-1</sup> and then of 18 m s<sup>-1</sup> ([Browning et al., 2010](#)). Interestingly, at no point in its lifetime did any significantly intense precipitation cells develop ahead of the NOSFX MCS as they did in CTL (Fig.s 10a and b). This suggests that the increase in velocity of the CTL MCS, corresponding to the phase when outflow reached the surface and generated new cells, was dependent more on the outflow reaching the surface than on the initiation of new convection.

#### *The vertical structure of the NOSFX MCS and its environment*

The NOSFX MCS was centred at 220 km at 1400 UTC (Figure 11a). A weak undercurrent remained in NOSFX between 230 and 290 km and which was about 750 m deep (Fig. 11a). Above the undercurrent was an elevated source layer centred at a height of about 1.5 km

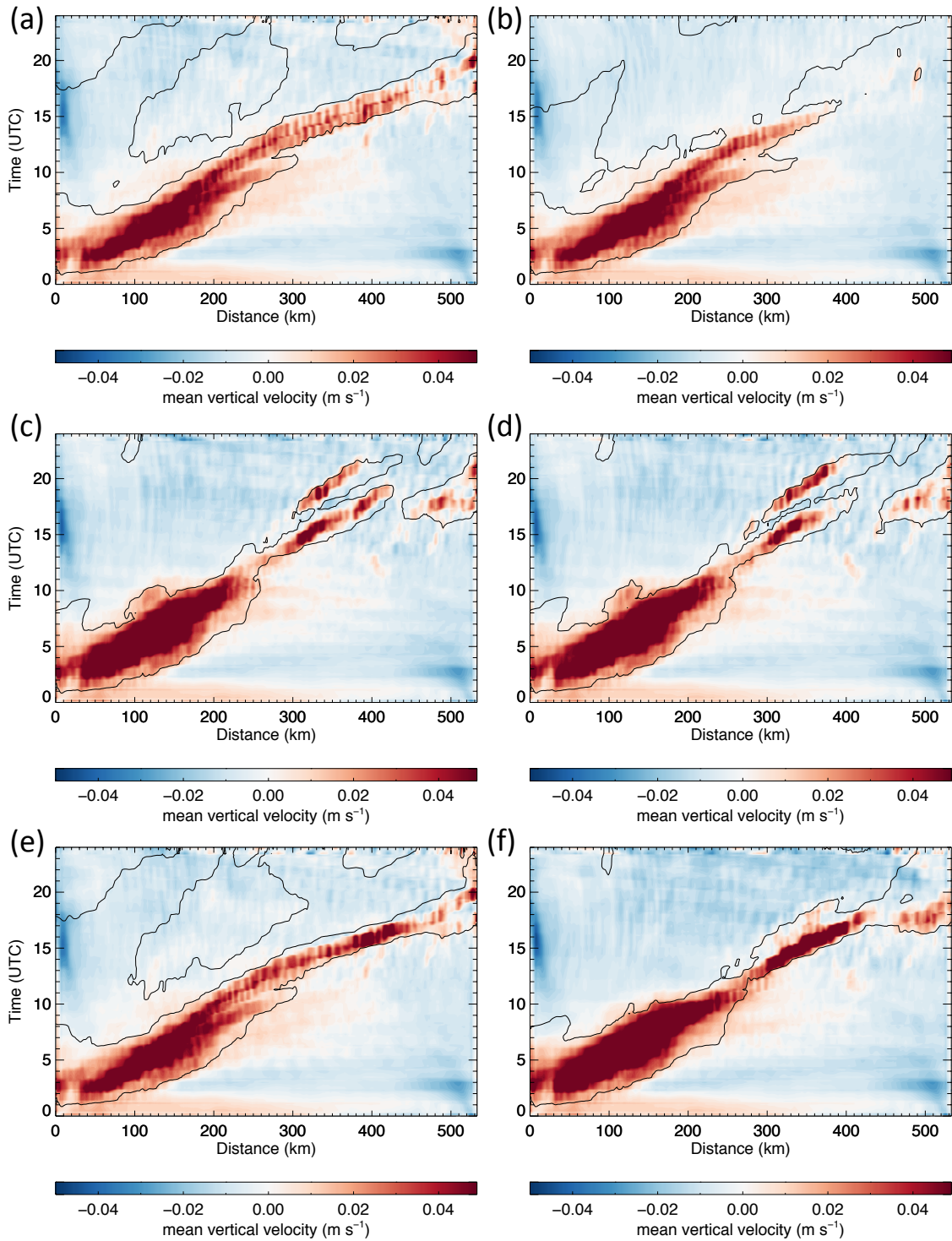


Figure 9: Zonally-averaged Hovmöller diagrams of column-mean vertical velocity ( $\text{m s}^{-1}$ , colour contour) and column-integrated total cloud at  $3.5 \text{ g kg}^{-1}$  (black line contour). from the inner domain of (a) CTL, (b) NOSFX, (c) NOEVP, (d) NOSUB, (e) NOMLT, and (f) NOCOOL. Distances are in km.

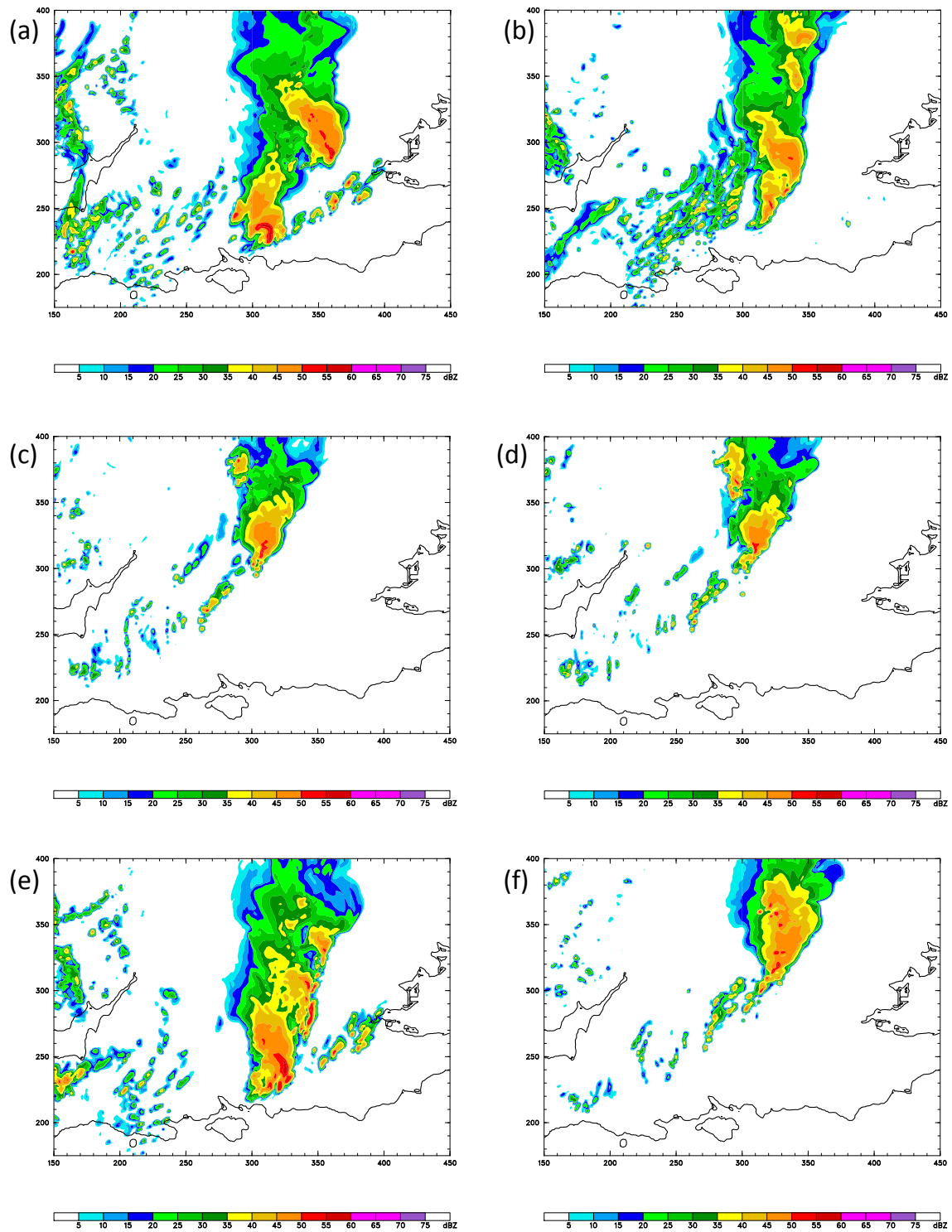


Figure 10: Simulated reflectivity (dBZ) field at 1400 UTC from the inner domain of (a) CTL, (b) NOSFX, (c) NOEVP, (d) NOSUB, (e) NOMLT, and (f) NOCOOL. Distances are in km.

(Fig. 11a). In contrast, no undercurrent was present in CTL at 1400 UTC and the inflow to the CTL MCS was from air with high  $\theta_e$  values originating from the surface (Fig. 11b). This is evidence that the surface heat fluxes weakened the undercurrent: removing the surface heat fluxes led to a longer-persisting undercurrent in NOSFX compared to CTL, prolonging the period of elevated convection in NOSFX.

Despite the persistence of the weak undercurrent in NOSFX, and the presence of the elevated inflow layer, there was also evidence that cold surface outflow was forming directly beneath the MCS in NOSFX at 1400 UTC (Fig. 11a). The descent of the low-valued  $\theta_e$  air coincided with an increase in speed of the NOSFX MCS, suggesting that the development of cold outflow may have been responsible for the increase in system velocity of the MCS. Trajectories (not shown) calculated 2 hours backwards from 1400 UTC and initialised in the cold-pool outflow showed that removing surface heating from the model led to a stronger, more persistent undercurrent in NOSFX that was less susceptible to penetration by air from the RIJ.

The cold outflow from the NOSFX MCS was not strong enough to initiate new convection at its leading edge, where there was no enhancement of low-level values of  $\theta_e$  by surface heating. The NOSFX storm was centred at 250 km at 1500 UTC (Fig. 11c), by which time almost no undercurrent remained and air with high values of  $\theta_e$  extended from the surface to about 2 km. Cold outflow about 1 km deep formed beneath the MCS (Fig. 11c). This cold outflow extended beneath the remaining elevated source layer to a region at 290 km where air near the surface had high values of  $\theta_e$ , but no new cells were initiated (Fig. 11c). In contrast, surface heating in CTL caused a greater increase in  $\theta_e$  at low-levels, allowing the outflow to initiate new deep convection 70 km ahead of the MCS. The CTL MCS was centred at 230 km at 1500 UTC (Fig. 11d) and cold outflow moved into a region of high-valued  $\theta_e$  air that originated from the surface. At the leading edge of the cold outflow (at 300 km) was a cell of deep convection extending from 1 km to a height of 12 km (Fig. 11d). This is evidence that surface heating led to the initiation of further deep convection in CTL and thus extending the lifetime of the MCS. In NOSFX no new cells of deep convection ever formed at the leading edge of its outflow, and the NOSFX MCS dissipated much earlier than the CTL MCS (Figs 9a,b).

### **Summary of the effects of surface heat fluxes on the simulated MCS:**

- By weakening the undercurrent, surface heating caused an earlier transition from elevated to surface-based convection in the simulation.
- The development of cold outflow from the NOSFX MCS coincided with an increase in speed despite the absence of secondary initiation.
- Surface heating enhanced the initiation of new deep convection from the surface and prolonged the lifetime of the MCS.

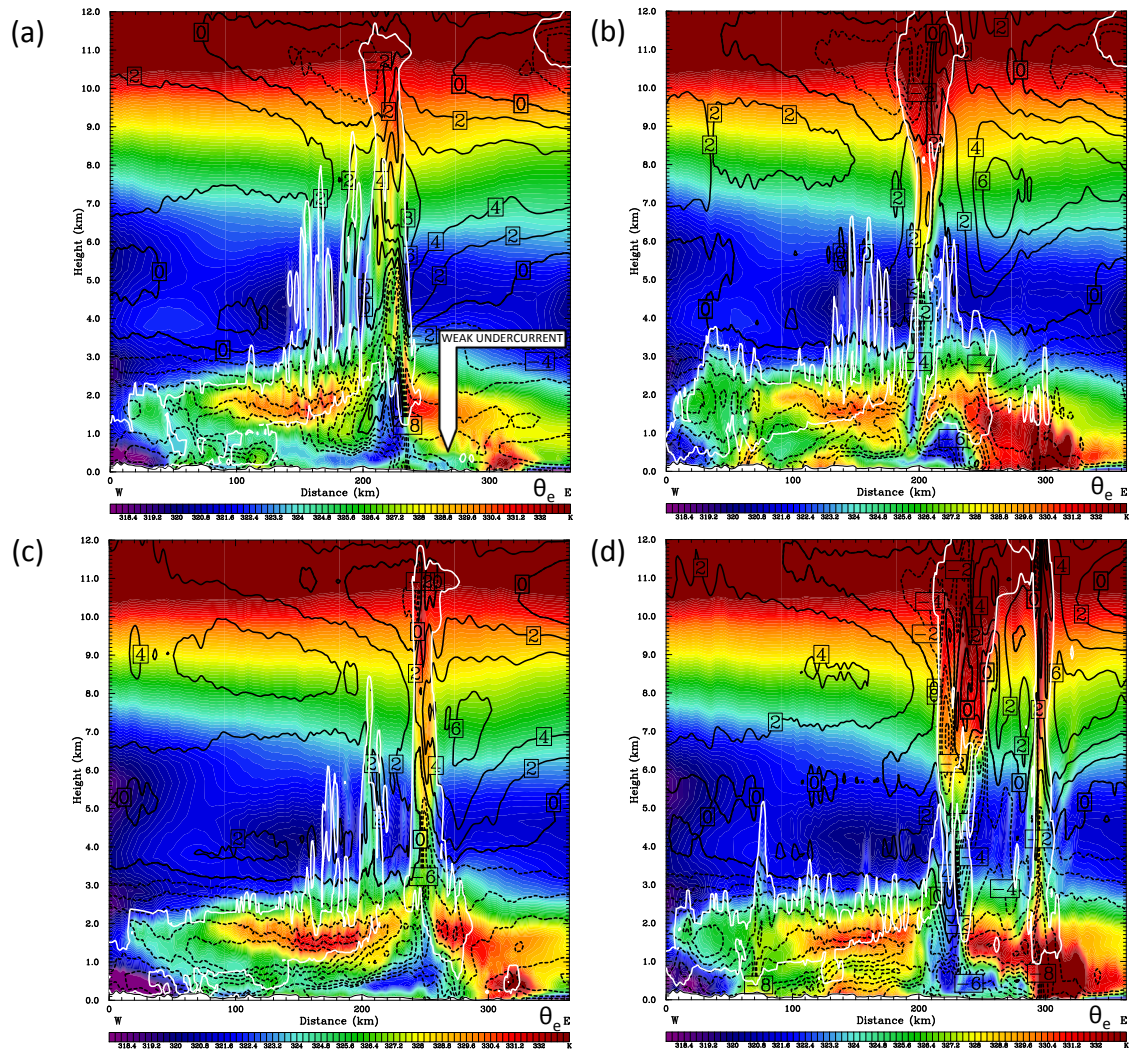


Figure 11: As Figure 4 but for (a,b) NOSFX, CTL at 1400 UTC and (c,d) NOSFX, CTL at 1500 UTC. An arrow labels the weak undercurrent in NOSFX at 1400 UTC in (a)

## 5.2 The dependence of the MCS on diabatic cooling from microphysical processes

### *The structure and evolution of the simulated precipitation*

Unlike the CTL MCS, the MCSs in NOEVP, NOSUB and NOCOOL had only one system velocity (Fig.s 9c,d and f), which were similar to the speed of the CTL system during its initial elevated phase (Table 2). Note that these runs also had stronger updraughts than CTL (Fig 9). It will be shown that the dynamical features of these systems did not evolve significantly, unlike the CTL run. Not surprisingly, evaporative and sublimational cooling had a much greater effect on the structure and evolution of the precipitation than cooling by melting (consistent with the findings of [Chen and Cotton, 1988](#)). Like CTL, the NOMLT MCS had two system velocities:  $6.5 \text{ m s}^{-1}$  during its initial phase, and  $12.4 \text{ m s}^{-1}$  from 1330 UTC onwards (Fig. 9e). These will be shown to correspond to the phases of convection before and after cold outflow reached the surface, as has already been shown in the case of the CTL run.

Cooling by evaporation and sublimation had a significant effect on the intensity of the simulated precipitation. When these processes were removed from the model the precipitation was weaker and less well-organised compared to CTL, propagated more to the northeast with the upper-level winds (Fig. 1d), and no intense cells ever developed ahead of the MCSs in NOEVP or NOSUB as they did in CTL (Fig.s 10a,c,d). In contrast, cooling by melting had a much weaker effect. The precipitation in NOMLT was more intense and better organised (Fig. 10e) and was more similar to that in CTL (Fig. 10a) than that in NOEVP or NOSUB (Fig.s 10c,d). Small cells of intense precipitation formed ahead of the MCS in NOMLT (Fig. 10e). It has been shown that these leading cells formed along an outflow boundary in CTL; we will show that this is true for NOMLT, and that the lack of new intense cells in NOEVP, NOSUB and NOCOOL is due to a lack of cold outflow in these runs.

### *The strengthening of the simulated undercurrent by diabatic cooling from microphysical processes*

System-relative flow at low-levels was towards the convective region at 0700 UTC in NOEVP, NOSUB and NOCOOL (Fig. 12a). In contrast, air with low values of  $\theta_e$  flowed at low levels out of the region of intense precipitation and ahead of the CTL storm (Fig. 12b). To the south of the MCS the cold outflow turned west, back towards the storm, providing an additional contribution to the cold air that flowed against the MCS. This shows that the early cold outflow that formed in the north of the MCS during the spin-up phase of CTL and NOMLT was driven by cooling from evaporation and sublimation, and that the cold outflow from the north acted to strengthen the undercurrent in the south. It is unknown whether diabatic cooling reinforced the observed undercurrent. The strengthening of the undercurrent caused southward elongation of the MCS (Fig.s 12c,d) likely due to increased lifting at the southern end of the MCS by the strengthened undercurrent. The cold outflow from the north also delayed the transition from elevated to surface-based convection (Fig.s 12c,d).

### *The effect of diabatic cooling from microphysical processes on the vertical structure of the*

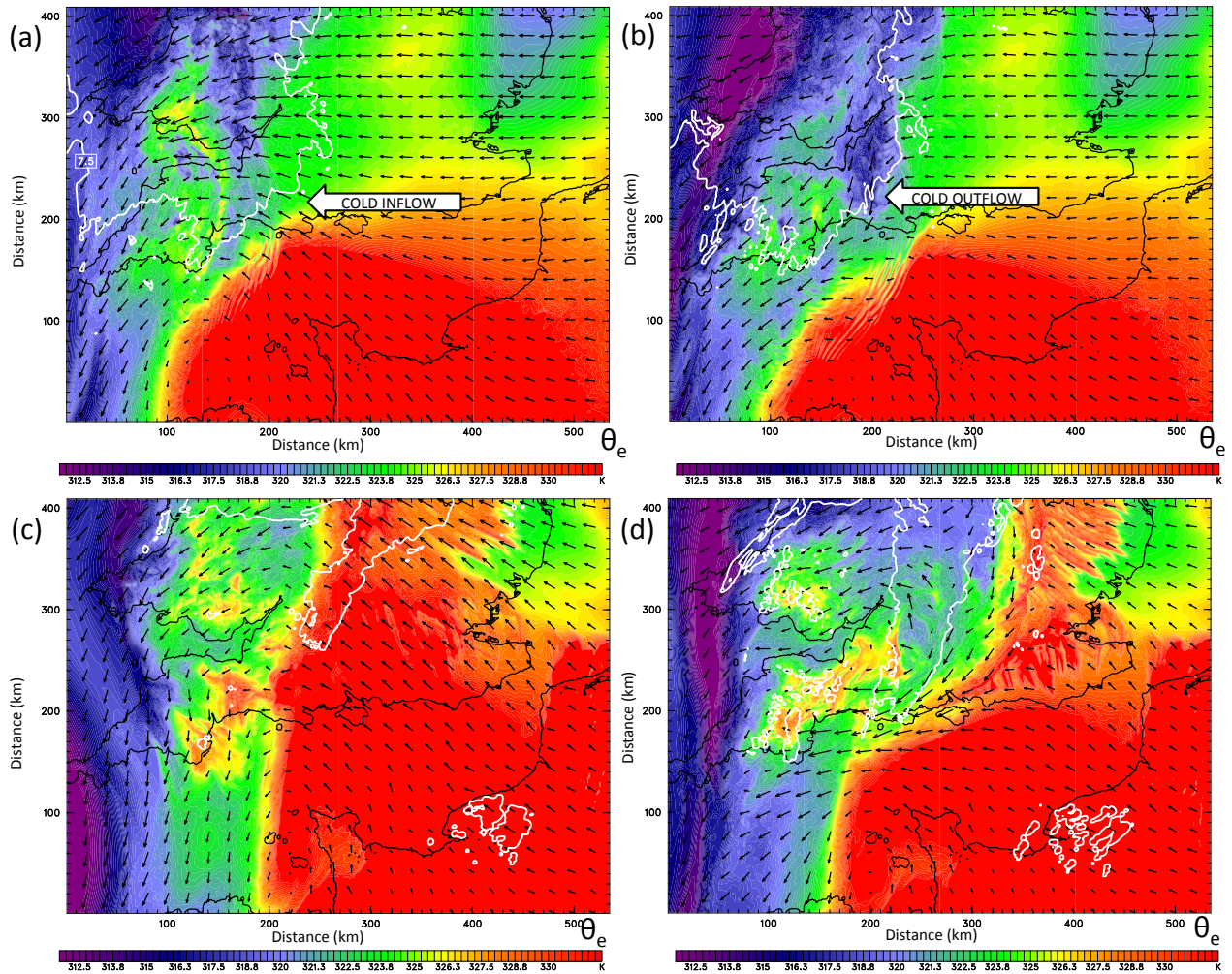


Figure 12:  $\theta_e$  (K, colour contour), maximum reflectivity in the column (dBZ, white line contour) and system-relative horizontal wind vectors at 950 hPa from the 1 km inner domain of (a,b) NOCOOL (also representing NOEVP and NOSUB) and CTL (also representing NOMLT) at 0700 UTC and (c,d) NOCOOL, CTL at 1200 UTC. Distances are in km. Note that the large-scale flow should be interpreted in a system-relative sense. Arrows label regions of cold inflow (a) and outflow (b).

### *simulated convection*

The inflow to the NOCOOL MCS (and also NOEVP and NOSUB) at 0815 UTC was from an elevated layer centred above an undercurrent (Fig. 13a). The RIJ in NOCOOL, with its rear edge centred at a height of about 4 km, only descended to about 2 km at 0815 UTC (Fig. 13a), whereas it reached 1 km in CTL (Fig. 13b). Even though the descent of the RIJ in NOCOOL was weak compared to CTL, and despite the shallower undercurrent, a wave formed in the elevated source layer at 0815 UTC and cloud formed ahead of the nose of the RIJ (Fig. 13a subpanel). The NOCOOL wave, however, only had one peak, whereas the CTL wave had four peaks at 0815 UTC (Fig. 13b subpanel), and the cloud associated with the CTL wave was much deeper than in NOCOOL (Fig. 13b). Without diabatic cooling this wave was much smaller, showing the role of diabatic cooling in the enhancement of the wave in this case (Marsham *et al.*, 2010) compared with diabatic heatings (Schumacher and Johnson, 2008). Without diabatic cooling the MCS persisted and the RIJ descended (similar to the results of Trier *et al.*, 2011), suggesting that diabatic heating and large-scale convergence (Crook and Moncrieff, 1988) may be key to maintaining convection in the absence of a cold pool.

Because the CTL undercurrent was strengthened by evaporation and sublimation, the removal of cooling by these processes meant that surface heating and the advection of high-valued  $\theta_e$  air in the east caused a significant increase in the values of  $\theta_e$  at low-levels ahead of the NOCOOL MCS (Fig. 13c and subpanel). There was no longer a wave in the elevated layer of high-valued  $\theta_e$  by 1030 UTC in NOCOOL (Fig. 13c subpanel), presumably because the absence of a low-level stable layer (the undercurrent) meant that wave-trapping could not occur. In contrast, the undercurrent was still present in CTL at this time, and the wave in the undercurrent had three distinct peaks (Fig. 13d and subpanel).

The RIJ in NOCOOL was always weaker than in CTL. It descended to an altitude of about 1.5 km at 1030 UTC in NOCOOL and 750 m in CTL (Figs 13c and d). The RIJ never penetrated to the surface in NOCOOL. That the RIJ descended at all in NOCOOL shows that the descent of the RIJ was partially caused by dynamic processes, in agreement with Schmidt and Cotton (1990); Pandya and Durran (1996); Trier *et al.* (2011). The descent was, however, strengthened by diabatic cooling processes. This is consistent with Braun (1995), who showed that the RIJ in their model was sensitive to latent cooling by sublimation, and also with the results of Yang and Houze (1995); Franklin *et al.* (2006); Clark *et al.* (2013a).

The effects of cooling by evaporation and sublimation were important not only in the RIJ, but also in the convective region. No cold outflow ever formed in NOCOOL, nor did any significant change in system velocity occur, confirming that the increase in system velocity in CTL was due to the formation of the cold outflow. The importance of evaporation and sublimation in the generation of cold outflow is consistent with the results of Yang and Houze (1995); Trier *et al.* (2011); Clark *et al.* (2013a), who all found that removing latent cooling either prevented or significantly weakened cold pool formation.

## Summary of the effects of diabatic cooling on the simulated MCS:

- Diabatic cooling from evaporation and sublimation caused the early formation of cold outflow in the spin-up phase of the CTL and NOMLT simulations, which had the following effects:
  1. The outflow turned back towards the storm and acted to strengthen the undercurrent directly.
  2. The outflow prolonged the period of elevated convection by reducing weakening of the undercurrent by advection of more buoyant air from the south of the domain.
- Cooling by evaporation and sublimation strengthened the descent of the RIJ and enhanced the formation of the wave during the elevated phase of convection.
- Cooling by sublimation and evaporation caused the development of the gravity current outflow.
- Without evaporational or sublimational cooling, the RIJ and the undercurrent were weaker and the convection did not remain wave-lifted for long.
- The generation of cold outflow by diabatic cooling processes coincided with the increase in speed of the simulated MCS during the surface-based convection phase.

## 6 Discussion

It is well-known that the stable layer beneath elevated convection is not dynamically passive. In the presence of a low-level stable layer a storm can generate features such as waves and bores that lift an elevated layer of air to its LFC, thereby maintaining convection (e.g. [Dudhia \*et al.\*, 1987](#); [Bosart and Seimon, 1988](#); [Crook and Moncrieff, 1988](#); [Schmidt and Cotton, 1990](#); [Buzzi \*et al.\*, 1991](#); [Fritsch and Forbes, 2001](#); [Stoelinga \*et al.\*, 2003](#); [Fovell \*et al.\*, 2006](#); [Schumacher and Johnson, 2008](#); [Parker, 2008](#); [Schumacher, 2009](#); [Marsham \*et al.\*, 2010, 2011](#)). However, this study provides a new insight into the nature of the stable layer that has not previously been noted in the literature: the stable layer beneath elevated storms is not necessarily independent of the convective processes. Early convective outflow from the north of the CTL MCS, cooled by evaporation and sublimation, acted to strengthen the undercurrent in the simulation, allowing wave-forced elevated convection to be maintained for a longer period than it was in the absence of such an outflow.

These simulations have confirmed the suggestion of [Browning \*et al.\* \(2010\)](#) that one possible mechanism for the generation of the wave was likely the interaction of the RIJ with the undercurrent. In this scenario there may be a positive feedback process between the convection, the RIJ and the stable layer. Diabatic cooling processes strengthen the descent of the RIJ (shown in this study, which is consistent with the findings of [Yang and Houze,](#)

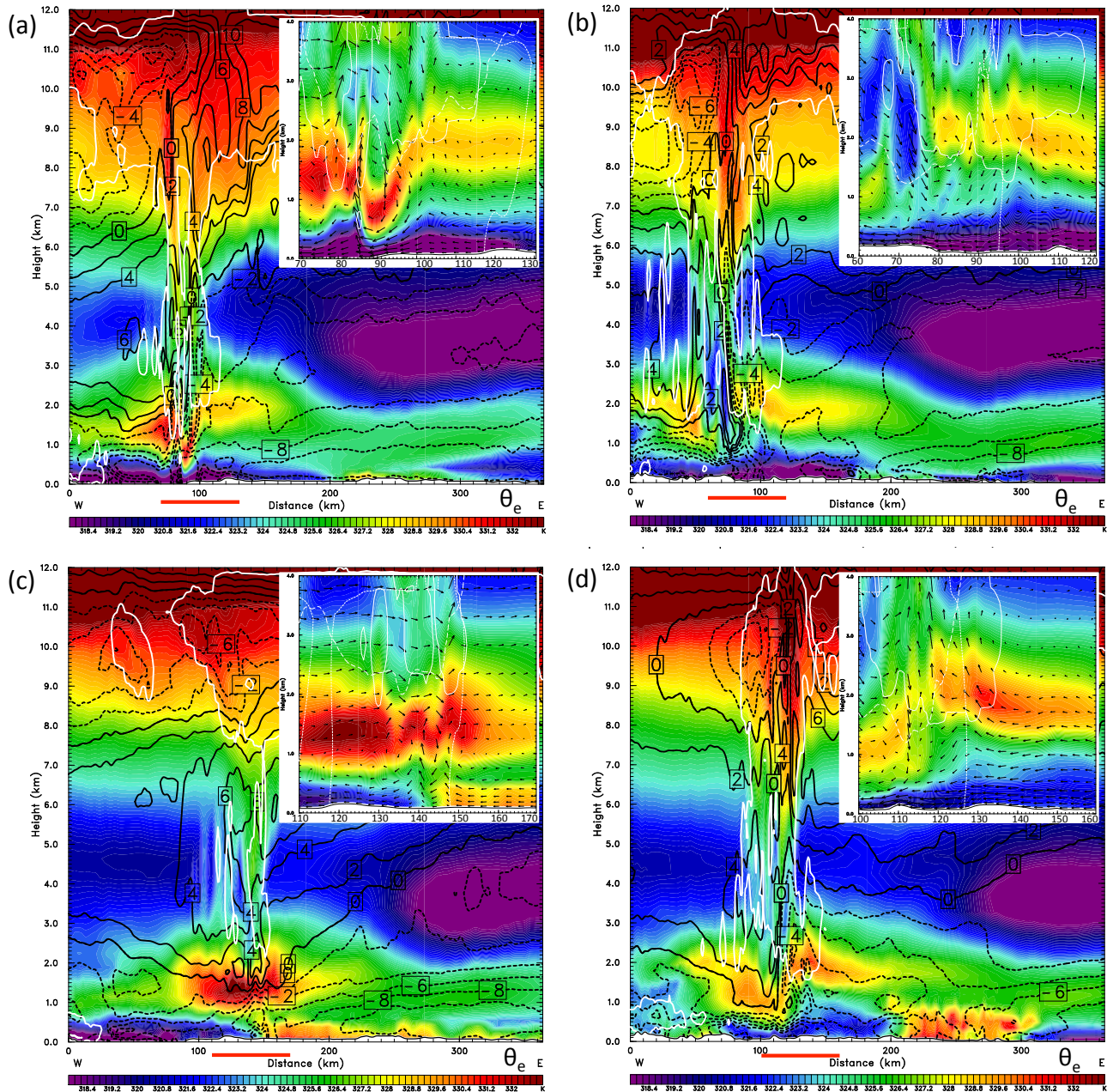


Figure 13: As Figure 4 but for (a,b) NOCOOL, CTL at 0815 and (c,d) NOCOOL, CTL at 1030 UTC. Note that due to the different geographical locations of the NOCOOL and CTL storms, the NOCOOL section does not have exactly the same location as the CTL section, but both are through the centre of the respective storms and are averaged by 10 km into and out of the plane of the section. The subpanels in the top right show detail of the region from heights of 0 to 4 km and along the 60 km horizontal sections shown by the red bars in the larger panels. The subpanels show  $\theta_e$  (colour contour, same scale as larger panels), system-relative 3D wind vectors resolved along the plane of the section and contour of the  $5 \times 10^{-3} \text{ g kg}^{-1}$  cloud, graupel and rain mixing ratio (solid, dashed and dotted white lines, respectively).

1995; Braun, 1995; Braun and Houze, 1997; Franklin *et al.*, 2006; Clark *et al.*, 2013a). A stronger RIJ may then generate a larger wave in the stable layer, which in turn may provide more lifting and lead to more intense convection. Stronger updrafts may lead to more ice particles being detrained to the stratiform region of cloud, so greater cooling can occur due to sublimation, causing a stronger RIJ. This suggests that there may be a critical strength of the RIJ and / or the wave for maintaining elevated deep convection. If the RIJ is too strong it will penetrate through the stable layer to the surface and either cause or strengthen cold outflow. Strong cold-pool outflow can lift near-surface air parcels, leading to a transition to surface-based convection. However, this study has also shown that microphysical cooling processes can strengthen the low-level stable layer, acting to maintain elevated convection for a longer period. The relative contributions of diabatic cooling to the maintenance of elevated convection via the reinforcement of the RIJ and via the strengthening of the undercurrent are at present unknown. It would be of interest to determine whether there is a positive feedback process in the storm such as that described above, and whether there is a critical strength of the RIJ for the maintenance of elevated deep convection.

## 7 Summary and Conclusions

This study provides an analysis of a simulated daytime elevated MCS with a RIJ occurring in the mid-latitude maritime climate of the UK and is one of very few published case-studies of elevated MCSs in the UK. Although there were differences between the CTL MCS and the observed CSIP IOP 3 MCS, the behaviour of the simulated system was close enough to reality for the model to be a useful tool to investigate the processes controlling the observed system. The work has shown that many factors can influence the maintenance of elevated deep convection occurring above a daytime stable layer, from the large-scale structure and flow of the atmosphere through to surface heating processes and cooling by evaporation and sublimation within the storm. Additionally, although the presence of a low-level stable layer is a known feature of elevated convection (e.g. Schmidt and Cotton, 1989; Wilson and Roberts, 2006), this work gives new insight into interactions and feedback mechanisms between the stable layer and the storm dynamics.

Several of the model results were similar to the observations of Browning *et al.* (2010): convection developed ahead of a cold front above a low-level, cold, stable undercurrent that flowed in the opposite direction to the MCS. However, there were also some differences: although several MCSs were observed, only one formed in the simulation; the undercurrent in the CTL simulation was about half of the observed 2-km depth; there was only one source layer with CAPE in the model, rather than two (which may be due to the model vertical resolution); and most significantly, the MCS in the simulation underwent a transition from elevated to surface-based convection (behaviour documented in other studies Trapp *et al.*, 2001; Bryan *et al.*, 2006; Corfidi *et al.*, 2008; Grim *et al.*, 2009; Marsham *et al.*, 2011; Trier *et al.*, 2011), while the IOP 3 MCS remained elevated throughout the observation period.

Convection and the RIJ formed during the model spin-up period so it was not possible to investigate the initiation from these simulations, but tests showed that diabatic cooling enhanced the RIJ (consistent with [Yang and Houze, 1995](#); [Braun, 1995](#); [Braun and Houze, 1997](#); [Franklin \*et al.\*, 2006](#); [Clark \*et al.\*, 2013a](#)). During the spin-up period diabatic cooling enhanced the undercurrent, and once the MCS formed the cooling enhanced the RIJ. As observed, the RIJ did not descend to the surface in CTL, but reached the top of the undercurrent, generating a wave. The structure of the flow resembled the bore described by the studies of [Parker \(2008\)](#) and [French and Parker \(2010\)](#) with the important difference that the low-level flow in their simulations was towards the storm, and even with the imposition of extra low-level jets experienced a stepwise increase in height as it interacted with the storm, not a stepwise decrease as occurred in our simulation. The feature in our simulation was therefore a wave. The wave aided triggering of convection and there appears to be a positive feedback between convection, the RIJ, the wave and triggering of new convection, as discussed above.

The transition of the CTL MCS from elevated to surface-based convection was similar to the evolution of the nocturnal squall line in the US Great Plains analysed by [Marshall \*et al.\* \(2011\)](#); [Trier \*et al.\* \(2011\)](#). However, those authors showed that the transition to surface-based convection only occurred after sunrise as the boundary layer warmed. In our CTL simulation, the undercurrent was not a nocturnal feature. Although the undercurrent was partly weakened by surface heating, advection of buoyant air from the south of the domain was an important factor that contributed to the transition to surface-based convection.

Surface latent and sensible heat fluxes affected the pre-convective environment by weakening the undercurrent and increasing the buoyancy of the near-surface air ahead of the MCS. This contributed to the transition to surface-based convection. The enhanced buoyancy of the near-surface pre-convective air also allowed secondary initiation by cold-pool outflow, which may have been responsible for increasing the lifetime of the system ([Wilson and Roberts, 2006](#)). The convective and environmental conditions were close to optimal for the generation of deep convection according to [Weisman and Rotunno \(2004\)](#). The development of the outflow coincided with a significant increase in system velocity of the storm, consistent with the results of [Schumacher \(2009\)](#), who found that rain propagation speeds increased when elevated systems became surface-based, and with [Trier \*et al.\* \(2011\)](#), who found that the horizontal speed of their simulated storm was much slower when latent cooling was removed and no outflow formed. It also appears that the increase in speed of the MCS was linked to the development of cold outflow rather than the initiation of new cells, as the speed of the NOSFX MCS increased when cold outflow formed even though no new initiation occurred.

It is interesting to contrast this case with the only other day during CSIP where an MCS was observed, where simulations captured a surface-based MCS much more accurately than the simulations of an elevated MCS presented here ([Clark \*et al.\*, 2013b,a](#)). It is likely that

the shallower-than-observed stable layer in our simulations was susceptible to penetration by downdraughts (Horgan *et al.*, 2007) and allowed the transition to a surface-based MCS with cold outflow, whereas this did not occur in the observations. In a simulation using the 1 km Met Office Unified Model the stable layer was even shallower than that in WRF and almost immediately the convection became surface-based, the RIJ reached the surface and a cold pool formed (not shown). This shows that accurately forecasting elevated convective systems depends critically on the representation of such stable layers, and therefore also on uncertainties in the synoptic scale.

## Acknowledgements

The authors thank all those who were involved in the CSIP project. The original CSIP project and the extended analysis phase leading to the present paper were funded under grants by the Natural Environment Research Council (NERC:NER/O/S/2002 00971 and NE/B505538/1). This work made use of the facilities of HECToR, the UK's national high-performance computing service, which was provided by UoE HPCx Ltd at the University of Edinburgh, Cray Inc and NAG Ltd, and funded by the Office of Science and Technology through EPSRC's High End Computing Programme. We thank two anonymous reviewers for thoughtful comments that helped to significantly improve this manuscript. Special thanks also go to Chris Dearden (University of Manchester, UK) for help with the WRF microphysics code, and to Doug Parker, Keith Browning (University of Leeds, UK), Alan Gadian and Ralph Burton (NCAS) for discussions which have helped to guide some of the work in the present paper. Rain rates retrieved from the UK network rain radars were provided by the Met Office.

## References

- Bennett L, Browning K, Blyth A, Parker D, Clark P. 2006. A review of the initiation of precipitating convection in the United Kingdom. *Quarterly Journal of the Royal Meteorological Society* **132**(617): 1001–1020.
- Bernardet L, Cotton W. 1998. Multiscale evolution of a derecho-producing mesoscale convective system. *Monthly Weather Review* **126**: 2991–3015.
- Bernardet L, Grasso L, Nachamkin J, Finley C, Cotton W. 2000. Simulated convective events using a high-resolution mesoscale model. *Journal of Geophysical Research* **105**: 14963–14982.
- Betts AK, Miller M. 1986. A new convective adjustment scheme. part II: Single column tests using GATE wave, BOMEX, ATEX, and Arctic Airmass data sets. *Quarterly Journal of the Meteorological Society* **112**: 693–710.
- Blanchard D. 1990. Mesoscale convective patterns of the southern high plains. *Bulletin American Meteorological Society* **71**: 994–1005.

- Bosart L, Seimon A. 1988. A case study of an unusually intense atmospheric gravity wave. *Monthly Weather Review* **116**: 1857–1886.
- Braun S. 1995. Multiscale process interactions associated with a midlatitude squall line. PhD thesis, University of Washington.
- Braun S, Houze Jr R. 1997. The evolution of the 10-11 June 1985 PRE-STORM squall line: Initiation, development of rear inflow, and dissipation. *Monthly Weather Review* **125**: 478–504.
- Browning K, Blyth A, Clark P, Corsmeier U, Morcrette C, Agnew J, Ballard S, Bamber D, Barthlott C, Bennett L, Beswick K, Bitter M, Bozier K, Brooks B, Collier C, Davies F, Deny B, Dixon M, Feuerle T, Forbes R, Gaffard C, Gray M, Hankers R, Hewison T, Kalthoff N, Khodayar S, Kohler M, Kottmeier C, Kraut S, Kunz M, Ladd D, Lean H, Lenfant J, Li Z, Marsham J, McGregor J, Mobbs S, Nicol J, Norton E, Parker D, Perry F, Ramatschi M, Ricketts H, Roberts N, Russell A, Schulz H, Slack E, Vaughan G, Waight J, Wareing D, Watson R, Webb A, Wieser A. 2007. The Convective Storm Initiation Project. *Bulletin American Meteorological Society* **88**: 1939–1955.
- Browning K, Hill F. 1984. Structure and evolution of a mesoscale convective system near the British Isles. *Quarterly Journal of the Meteorological Society* **110**: 897–913.
- Browning KA, Marsham JH, Nicol JC, Perry FM, White BA, Blyth AM, Mobbs SD. 2010. Observations of dual slantwise circulations above a cool undercurrent in a mesoscale convective system. *Quarterly Journal of the Royal Meteorological Society* **136**: 354–373.
- Browning KA, Marsham JH, White BA, Nicol JC. 2012. A case study of a large patch of billows surmounted by elevated convection. *Quarterly Journal of the Royal Meteorological Society* **138**.
- Bryan G, Knievel J, Parker M. 2006. A multimodel assessment of RKW theory’s relevance to squall-line characteristics. *Monthly Weather Review* **134**: 2772–2773.
- Buzzi A, Fantini M, Lippolis G. 1991. Quasi-stationary organized convection in the presence of an inversion near the surface: experiments with a 2-D numerical model. *Meteorology and Atmospheric Physics* **45**: 75–86.
- Charba J. 1974. Application of gravity current model to analysis of squall-line gust front. *Monthly Weather Review* **102**: 140–156.
- Chen S, Cotton W. 1988. The sensitivity of a simulated extratropical mesoscale convective system to longwave radiation and ice-phase microphysics. *Journal of the Atmospheric Sciences* **45**: 3897–3910.
- Chong M, Amayenc P, Scialom G, Testud J. 1987. A tropical squall line observed during the COPT 81 experiment in West Africa. Part I: Kinematic structure inferred from dual-Doppler radar data. *Monthly Weather Review* **115**: 670–694.
- Clark P, Browning K, Forbes R, Morcrette C, Blyth A, Lean H. 2013a. The evolution of an MCS over southern England. Part II: Model simulations and sensitivity to microphysics. *Quarterly Journal of the Royal Meteorological Society* .
- Clark P, Browning K, Morcrette C, Blyth A, Forbes R, Brooks B, Perry F. 2013b. The evolution of an MCS over southern England. Part I: Observations. *Quarterly Journal of the Royal Meteorological Society* .

- Colman B. 1990. Thunderstorms above frontal surfaces in environments without positive CAPE. Part I: A climatology. *Monthly Weather Review* **118**: 1103–1122.
- Coniglio M, Correia Jr J, Marsh P, Kong F. 2013. Verification of convection-allowing WRF model forecasts of the planetary boundary layer using sounding observations. *Weather and Forecasting* **28**: 842862.
- Corfidi S, Corfidi S, Schultz D. 2008. Elevated convection and castellanus: Ambiguities, significance, and questions. *Weather and Forecasting* **23**: 1280–1302.
- Cotton W, George R, Wetzel P, McAnelly R. 1983. A long-lived mesoscale convective complex. Part I: The mountain-generated component. *Monthly Weather Review* **111**: 1893–1918.
- Cotton W, Lin MS, McAnelly R, Tremback C. 1989. A composite model of mesoscale convective complexes. *Monthly Weather Review* **117**: 765783.
- Crook N, Moncrieff M. 1988. The effect of large-scale convergence on the generation and maintenance of deep moist convection. *Journal of the Atmospheric Sciences* **45**: 3606–3624.
- Davis C, Manning K, Carbone R, Trier S, Tuttle J. 2003. Coherence of warm-season continental rainfall in numerical weather prediction models. *Monthly Weather Review* **131**: 26672679.
- Dudhia J. 1989. Numerical study of convection observed during the winter monsoon experiment using a mesoscale two-dimensional model. *Journal of the Atmospheric Sciences* **46**: 3077–3107.
- Dudhia J, Moncrieff M, So D. 1987. The two-dimensional dynamics of West African squall lines. *Quarterly Journal of the Royal Meteorological Society* **113**: 121–146.
- Fovell R, Mullendore G, Kim S. 2006. Discrete propagation in numerically simulated nocturnal squall lines. *Monthly Weather Review* **134**: 3735–3752.
- Franklin C, Holland G, May P. 2006. Mechanisms for the generation of mesoscale vorticity features in tropical cyclone rainbands. *Monthly Weather Review* **134**: 2649–2669.
- French A, Parker M. 2010. The response of simulated nocturnal convective systems to a developing low-level jet. *Journal of the Atmospheric Sciences* **67**: 3384–3408.
- Fritsch J, Forbes G. 2001. Mesoscale convective systems. *Severe Convective Storms, Meteorological Monographs* (50): 323–358.
- Fritsch J, Maddox R. 1981. Convectively driven mesoscale weather systems aloft. Part I: Observations. *Journal of Applied Meteorology* **20**: 919.
- Glickman T. 2000. *Glossary of Meteorology*. American Meteorological Society, second edn.
- Goff R. 1976. Vertical structure of thunderstorm outflows. *Monthly Weather Review* **104**: 1429–1440.
- Goss S, Thompson R, Bookbinder E. 2006. An elevated supercell with damaging wind from the morning of 12 March 2006. In: *23<sup>rd</sup> Conference on Severe Local Storms*.
- Grim J, Rauber R, McFarquhar G, Jewett B. 2009. Development and forcing of the rear inflow jet in a rapidly developing and decaying squall line during BAMEX. *Monthly Weather Review* **137**: 1206–1229.

- Hong S, Noh Y, Dudhia J. 2006. A new vertical diffusion package with an explicit treatment of entrainment processes. *Monthly Weather Review* **134**: 2318-2341.
- Hong SY, Dudhia J. 2012. Next-generation numerical weather prediction: Bridging parameterization, explicit clouds, and large eddies. *Bulletin American Meteorological Society* **93**: ES6-ES9.
- Horgan K, Schultz D, Hales Jr J, Corfidi S, Johns R. 2007. A five-year climatology of elevated severe convective storms in the United States east of the Rocky Mountains. *Weather and Forecasting* **22**: 1031-1044.
- Houze Jr RA, Rutledge S, Biggerstaff M, Smull B. 1989. Interpretation of Doppler Weather Radar Displays of Midlatitude Mesoscale Convective Systems. *Bulletin American Meteorological Society* **70**(6): 608-619.
- Hu XM, Nielsen-Gammon J, Zhang F. 2010. Evaluation of three planetary boundary layer schemes in the WRF model. *Journal of Applied Meteorology and Climatology* **49**: 1831-1844.
- Janjić Z. 2000. Comments on 'development and evaluation of a convection scheme for use in climate models'. *Journal of the Atmospheric Sciences* **57**: 3686.
- Janjić ZI. 1990. The step-mountain coordinate: Physical package. *Monthly Weather Review* **118**: 1429-1443.
- Janjić ZI. 1994. The step-mountain eta coordinate model: Further developments of the convection, viscous sublayer and turbulence closure schemes. *Monthly Weather Review* **122**: 927-945.
- Janjić ZI. 2002. Nonsingular implementation of the Mellor-Yamada level 2.5 scheme in the NCEP meso model. *NCEP Office Note* (437): 61.
- Lafore J, Moncrieff M. 1989. A numerical investigation of the organization and interaction of the convective and stratiform regions of tropical squall lines. *Journal of the Atmospheric Sciences* **46**: 521-544.
- Laing A, Fritsch J. 1997. The global population of mesoscale convective complexes. *Quarterly Journal of the Royal Meteorological Society* **123**: 389-405.
- Lin Y, Deal R, Kulie M. 1998. Mechanisms of cell regeneration, development, and propagation within a two-dimensional multicell storm. *Journal of the Atmospheric Sciences* **55**: 1867-1886.
- Maddox R. 1983. Large-scale meteorological conditions associated with midlatitude, mesoscale convective complexes. *Monthly Weather Review* **111**: 1475-1493.
- Marsham J, Browning K, Parker D, Norton E, Blyth A, Corsmeier U, Perry F. 2010. Multi-sensor observations of a wave beneath an impacting rear-inflow jet in an elevated mesoscale convective system. *Quarterly Journal of the Royal Meteorological Society* **136**: 1788-1812.
- Marsham J, Trier S, Weckwerth T, Wilson J. 2011. Observations of elevated convection initiation leading to a surface-based squall line during 13 June IHOP\_2002. *Monthly Weather Review* **139**: 247-271.
- Mellor G, Yamada T. 1982. Development of a turbulent closure model for geophysical fluid problems. *Reviews of Geophysics and Space Physics* **20**: 851-875.

- Mlawer EJ, Taubman SJ, Brown PD, Iacono MJ, Clough SA. 1997. Radiative transfer for inhomogeneous atmosphere: RRTM, a validated correlated-k model for the longwave. *Journal of Geophysical Research* **102**: 16 663–16 682.
- Moore J, Czarnetzki A, Market P. 1998. Heavy precipitation associated with elevated thunderstorms in a convectively unstable layer aloft. *Meteorological Applications* **5**: 373–384.
- Moore J, Glass F, Graves C, Rochette S, Singer M. 2003. The environment of warm-season elevated thunderstorms associated with heavy rainfall over the central United States. *Weather and Forecasting* **18**: 861–878.
- Morcrette C, Browning K, Blyth A, Bozier K, Clark P, Ladd D, Norton E, Pavelin E. 2006. Secondary initiation of multiple bands of cumulonimbus over southern Britain. I: An observational case-study. *Quarterly Journal of the Royal Meteorological Society* **132**: 1021–1051.
- Morrison H CJ, Khvorostyanov V. 2005. A new double-moment microphysics parameterization for application in cloud and climate models. Part I : Description. *Journal of the Atmospheric Sciences* **62**: 1665–1677.
- Morrison H, Thompson G, Tatarskii V. 2009. Impact of cloud microphysics on the development of trailing stratiform precipitation in a simulated squall line: Comparison of one- and two-moment schemes. *Mon. Wea. Rev.* **137**: 991–1007, doi:10.1175/2008MWR2556.1.
- Mueller C, Carbone R. 1987. Dynamics of a thunderstorm outflow. *Journal of the Atmospheric Sciences* **44**: 1879–1898.
- Ogura Y, Liou M. 1980. The structure of a midlatitude squall line: A case study. *Journal of the Atmospheric Sciences* **37**: 553–567.
- Pandya R, Durran D. 1996. The influence of convectively generated thermal forcing on the mesoscale circulation around squall lines. *Journal of the Atmospheric Sciences* **53**: 2924–2951.
- Parker M. 2008. Response of simulated squall lines to low-level cooling. *Journal of the Atmospheric Sciences* **65**: 1323–1341.
- Parker M, Johnson R. 2000. Organizational modes of midlatitude mesoscale convective systems. *Monthly Weather Review* **128**: 3413–3436.
- Rochette S, Moore J. 1996. Initiation of an elevated mesoscale convective system associated with heavy rainfall. *Weather and Forecasting* **11**: 443–457.
- Rotunno R, Klemp J, Weisman M. 1988. A theory for strong, long-lived squall lines. *Journal of the Atmospheric Sciences* **45**: 463–485.
- Rutledge S, Houze Jr R, Biggerstaff M, Matejka T. 1988. The Oklahoma-Kansas mesoscale convective system of 10–11 June 1985: Precipitation structure and single-Doppler radar analysis. *Monthly Weather Review* **116**: 1409–1430.
- Schmidt J, Cotton W. 1989. A high plains squall line associated with severe surface winds. *Journal of the Atmospheric Sciences* **46**(3): 281–302.
- Schmidt J, Cotton W. 1990. Interactions between upper and lower tropospheric gravity waves on squall line structure and maintenance. *Journal of the Atmospheric Sciences* **47**: 1205–1222.

- Schumacher R. 2009. Mechanisms for quasi-stationary behaviour in simulated heavy-rain-producing convective systems. *Journal of the Atmospheric Sciences* **66**: 1543–1568.
- Schumacher R, Johnson R. 2008. Mesoscale processes contributing to extreme rainfall in a midlatitude warm-season flash flood. *Monthly Weather Review* **136**: 3964–3986.
- Shin H, Hong SY. 2011. Intercomparison of planetary boundary-layer parametrizations in the wrf model for a single day from cases-99. *Boundary-Layer Meteorology* **139**(2): 261–281.
- Simpson J. 1969. A comparison between laboratory and atmospheric density currents. *Quarterly Journal of the Royal Meteorological Society* **95**: 758–765.
- Skamarock W, Klemp J, Dudhia J, Gill D, Barker D, Duda M, Huang X, Wang W, Powers J. 2008. A description of the advanced research WRF version 3 NCAR technical note June 2008. Technical Report TN-475+STR, NCAR.
- Smull B, Houze Jr R. 1985. A midlatitude squall line with a trailing region of stratiform rain: Radar and satellite observations. *Monthly Weather Review* **113**: 117–133.
- Smull B, Houze Jr R. 1987a. Dual-doppler radar analysis of a midlatitude squall line with a trailing region of stratiform rain. *Journal of the Atmospheric Sciences* **44**: 2128–2149.
- Smull B, Houze Jr R. 1987b. Rear inflow in squall lines with trailing stratiform precipitation. *Monthly Weather Review* **115**: 2869–2889.
- Stoelinga M, Locatelli J, Schwartz R, Hobbs P. 2003. Is a cold pool necessary for the maintenance of a squall line produced by a cold front aloft? *Monthly Weather Review* **131**: 95–115.
- Trapp R, Schultz D, Ryzhkov V, Holle R. 2001. Multiscale structure and evolution of an Oklahoma winter precipitation event. *Monthly Weather Review* **129**: 486–501.
- Trier S, Davis C, Ahijevych D, Weisman M, Bryan G. 2006. Mechanisms supporting long-lived episodes of propagating nocturnal convection within a 7-day WRF model simulation. *Journal of the Atmospheric Sciences* **63**: 2437–2461.
- Trier S, Marsham J, Davis C, Ahijevych D. 2011. Numerical simulations of the post-sunrise reorganization of a nocturnal mesoscale convective system during 13 June IHOP\_2002. *Journal of the Atmospheric Sciences* **68**: 2988–3011.
- Wakimoto RM. 1982. The life cycle of thunderstorm gust fronts as viewed with Doppler radar and rawinsonde data. *Monthly Weather Review* **110**: 1060–1082.
- Weisman M, Rotunno R. 2004. “A theory for strong long-lived squall lines” revisited. *Journal of the Atmospheric Sciences* **61**: 361–382.
- Wetzel P, Cotton W, McAnelly R. 1983. A long-lived mesoscale convective complex. Part II: Evolution and structure of the mature complex. *Monthly Weather Review* **111**: 1919–1937.
- Wilson J, Roberts R. 2006. Summary of convective storm initiation and evolution during IHOP: Observational and modelling perspective. *Monthly Weather Review* **134**: 23–47.
- Wilson J, Schreiber W. 1986. Initiation of convective storms at radar-observed boundary-layer convergence lines. *Monthly Weather Review* **114**: 2516–2536.
- Wyngaard J. 2004. Toward numerical modeling in the terra incognita. *Journal of the Atmospheric Sciences* **61**: 1816–1826.
- Xie B, Fung JCH, Chan A, Lau A. 2012. Evaluation of nonlocal and local planetary boundary

- layer schemes in the wrf model. *Journal of Geophysical Research: Atmospheres* **117**(D12).
- Yang M, Houze Jr R. 1995. Sensitivity of squall-line rear inflow to ice microphysics and environmental humidity. *Monthly Weather Review* **123**: 3175–3193.
- Zhang D, Gao K. 1989. Numerical simulation of an intense squall line during 10-11 June 1985 PRE-STORM. part II: Rear inflow, surface pressure perturbations and stratiform precipitation. *Monthly Weather Review* **117**: 2067–2094.